Robust Tactile Descriptors for Discriminating Objects From Textural Properties via Artificial Robotic Skin

Mohsen Kaboli and Gordon Cheng, *Fellow, IEEE*

***Abstract*—In this paper, we propose a set of novel tactile descriptors to enable robotic systems to extract robust tactile information during tactile object explorations, regardless of the number of the tactile sensors, sensing technologies, type of exploratory movements, and duration of the objects' surface exploration. The performance and robustness of the tactile descriptors are verified by testing on four different sensing technologies (dynamic pressure sensors, accelerometers, capacitive sensors, and impedance electrode arrays) with two robotic platforms (one anthropomorphic hand and one humanoid), and with a large set of objects and materials. Using our proposed tactile descriptors, the Shadow Hand, which has multimodal robotic skin on its fingertips, successfully classified 120 materials (100% accuracy) and 30 in-hand objects (98% accuracy) with regular and irregular textural structure by executing human-like active exploratory movements on their surface. The robustness of the proposed descriptors was assessed further during the large object discrimination with a humanoid. With a large sensing area on its upper body, the humanoid classified 120 large objects with multiple weights and various textures while the objects slid between its sensitive hands, arms, and chest. The achieved 90% recognition rate shows that the proposed tactile descriptors provided robust tactile information from the large number of tactile signals for identifying large objects via their surface texture regardless of their weight.**

***Index Terms*—Electronic skin, tactile feature descriptors, tactile sensing.**

I. Introduction

HUMANS rely on sense of touch for perception and control of the body, grasping, manipulating, and identifying objects via their physical properties, such as texture, shape, and stiffness [1]. For robotic systems that interact with dynamic environments, recognizing object properties is a crucial but difficult task for advanced vision techniques due to occlusion, poor lighting situations, and a lack of precision. Tactile sensing instead can provide a rich and direct feedback with the robotic systems from multiple contact points and a large tactile sensing area [2], [3].

Developing tactile sensing for the robotic systems has been investigated for several decades. Over the last decade, tactile sensing devices have evolved from being located on a fingertip to full hand and even whole body of robots [4].

In this regard, many tactile sensors with various sensing principles and technologies, e.g., resistive [5], [6], capacitive [7]–[9], optical [10], [11], piezoelectric [12], [13], acoustic [14], [15], recently organic bendable and stretchable [16], [17], etc., have been proposed.

In contrary to the rapid progress of tactile sensor advancement, considerably less attention has been given to research in tactile perception, tactile information processing, and tactile learning. In other words, the performance of tactile systems depends not only on the technological aspects of sensory devices, but also on the design of feature descriptors and learning methods that robustly extract and interpret the information contained in tactile data.

The physical object characteristics can be divided into three general classes: geometric information, inner properties (e.x. center of mass), and material properties. The geometric properties can be recognized by object size and shape via proprioceptive receptors, and related works in the area of robotics can be found in [18] and [19].

The center of mass of rigid objects is determined by lifting object from different objects' positions [20], [21]. The objects' material can be characterized by stiffness, thermal conductivity, and textural properties [22].

The perception of the textural properties of objects is one the most challenging task. The objects' texture can be sensed through the cutaneous tactile receptors while moving fingertips or even any sensitive parts of body on the surface of the objects (active touch) or when objects move on a sensitive skin area (passive touch). Tactile object discrimination by means of textural properties is a difficult and challenging task in robotics.

In this paper, we focus on the design of a set of novel tactile descriptor in order to extract robust features from the generated raw tactile signals (both stationary and nonstationary tactile signals) during tactile object exploration regardless of the number of tactile sensors (large-scale robotic skin) and their sensing technologies. The proposed tactile descriptors are invariant with respect to specific exploratory movements and their corresponding parameters (such as exploration time).

A. Background

Previously, customized simple tools or robotic end-effectors with various tactile sensors have been used to discriminate among objects via their textural properties. For instance, Dallaire *et al.* [23] managed to classify 28 different surfaces such

Manuscript received July 13, 2017; revised December 14, 2017; accepted February 18, 2018. Date of publication July 6, 2018; date of current version August 15, 2018. This paper was recommended for publication by Associate Editor R. Dahiya and Editor A. Billard upon evaluation of the reviewers' comments. This work is supported by the European Commission under Grant PITN-GA-2012-317488-CONTEST. *(Corresponding author: Mohsen Kaboli.)*

The authors are with the Institute for Cognitive Systems (ICS), Technische Universität München, Mnchen 80333, Germany (e-mail: mohsen.kaboli@tum.de; gordon.cheng@ieee.org).

Color versions of one or more of the figures in this paper are available online at http://ieeexplore.ieee.org.

Digital Object Identifier 10.1109/TRO.2018.2830364

1552-3098 © 2018 IEEE. Translations and content mining are permitted for academic research only. Personal use is also permitted, but republication/redistribution requires IEEE permission. See http://www.ieee.org/publications_standards/publications/rights/index.html for more information.

as aluminum, Plexiglas, kitchen towel, etc., with 90% accuracy with SVM and Pitman–Yor process algorithms. To do this, a three-axis accelerometer was placed on a stylus, which was then mounted above a well-controlled rotating table on which the surface was placed. Here, in order to generate tactile features, a set of parameters including variance, skewness, kurtosis, fifth moment, sum of the variation over time, and sum of higher half of amplitude spectrum were computed from the recorded data. The same parameters have been used in [24] to differentiate ten different indoor and outdoor surfaces from each other. In this study, an accelerometer mounted on a probe was employed to slide over experimental surfaces, such as wooden flooring, short hair carpet, and linoleum tile flooring. The authors reported the classification rate of 89.9% and 94.6% with 1 s and 4 s time windows of data, respectively.

In another work, in order to classify seven wooden surfaces, in [25] Chathuranga *et al.* used a biomimetic fingertip with three commercial accelerometers and seven force sensors, which was then fixed to a horizontal linear stage. In this experiment, in order to collect data, the artificial fingertip moved forward and backward on the wooden surfaces with a half second pause between each single movement. The applied vertical force and the velocity of movement were kept constant during the entire training and testing data collection procedure. In this paper, three feature parameters, including wavelet energy, variance of approximate signal, and mean of approximate signal were calculated from the recorded tactile signals. Using an artificial neural network, the authors classified seven wooden surfaces with a 65% success rate.

Jamali and Sammut [26] fabricated a bio-mimetic sensor made of silicon, within which were two polyvinylidene difluoride (PVDF) pressure sensors and two strain gauges. The finger was mounted on a robotic gripper and scraped over eight materials to classify the test surfaces. Fourier transform as a feature descriptor and various learning algorithms have been used to find the optimal technique for the texture recognition problem. In this paper, the feature descriptor heavily depends on the applied force and sliding duration. Moreover, it can only identify materials with a periodic texture structure. In another research study [27], the BioTac sensor was mounted on a linear stage to classify 117 different textures. Features like roughness, fineness, and traction were identified from the literature on human perception, and then modeled analytically. Although the authors reported a 95.4% classification rate, the proposed features are highly sensitive to the small variation in sliding time and velocity. Sinapov *et al.* used a humanoid with a three-axis accelerometer mounted on an artificial fingernail to classify 20 different uniform textures. In this instance, the robot scratched on the experimental surfaces with a controlled applied force, fixed velocities, and well-defined scratching movements. Faster scratches usually ended up having higher recognition accuracy. Additionally, combining the result of multiple scratches was more accurate than only performing a single scratch [28]. Here, a discretized spectrogram was used as feature descriptors for surface classification task [28]. Recently, in [29] Xu *et al.* used the Shadow Hand with the BioTac sensor on its index finger to execute exploratory movements over an object's surface; *pressure* to obtain flexibility information, *sliding* to obtain vibro-tactile information, and *contact* to measure heat flow. However, in this study, the base and wrist of the dexterous robotic hand were fixed on a table, and all joints in the hand and wrist were deactivated (except for two joints of the index finger). This was done to stabilize the system and to prevent the effect of the noise coming from the hand motion and motor vibration on the sensed tactile data. This constraint results in an unnatural and unscalable method of exploration; our study instead removes this restriction and allows for a more natural and human-like texture exploration using the Shadow Hand with all its fingers. Moreover, in order to differentiate objects from each other via textural properties, the authors considered only the data that were recorded during the middle of the sliding movements, and the contribution of the generated vibro-tactile signal at the start of the sliding as well as at the end of the movements were eliminated.

Chu *et al.* [30] used the PR2 robot with two BioTac sensors on its gripper to classify 60 objects via their physical properties, such as stiffness, temperature, volume, and textures. In this case, the robot applied a series of five predefined well-controlled exploratory motions on each of the 60 experimental objects: tap; squeeze; static hold, slow slide, and fast slide. The researchers, computed two set of features called static feature and dynamic feature. To generate static features they computed mean and maximum value of the low-frequency signal measured by the BioTac. In addition, they converted the recorded high-frequency signals into a nonnormalized energy spectral density (ESD). To represent the ESD via single-valued feature, they calculated the total energy of the ESD curve, plus the spectral centroid, variance, skewness, and kurtosis. To obtain the dynamic features, they used hidden Markov models to capture the variations in the recorded tactile data followed by three preprocessing steps. The static and dynamic features had 188 and 16 elements, respectively. The proposed method showed promise in object recognition via multiple physical properties, such as stiffness, temperature, volume, and texture using two tactile sensors. However, the author did not evaluate the performance of their method neither with single physical property nor with a large-scale robotic skin.

To tackle surface texture classification problems in [31], a force sensor, an accelerometer, and a position-orientation sensor were used to develop a haptic tool that was then utilized by a robotic hand to identify surface textures. The exploratory action was a sliding of the tool over the surface with constant velocity and normal force. Another related work was conducted by Watanabe *et al.* in which the authors tried to differentiate various kinds of papers from each other via the pushing and sliding of a tactile sensor on the papers [32]. To do this, the authors fabricated a tactile sensor consisting of microcantilevers with a strain gauge film on Si. The sensor was then fixed on a X–Y stage, and a six-axis force sensor on a jig was mounted under the Z stage. A set of actions like pushing and sliding with constant velocity and force were applied to explore the properties of various papers.

In another work, five textiles were explored and classified during an active sliding with constant velocity and through an array of Micro-Electro-Mechanical Systems (MEMS) in the distal phalanx of a robotic finger [33]. In order to classify four ob-

jects, in [34] Tanaka *et al.* used the Shadow Hand with three BioTac sensors and an active learning approach in which a latent variable estimation is carried out to learn individual object models. The exploratory motions were selected by the robot while modifying the parameters to dynamic motion primitively. The authors utilized stiffness, temperature, and textural properties to identify six objects. However, the proposed method has high computational complexity. In [35], a robotic arm equipped with accelerometers was used to classify 18 metal surfaces. In this scenario, tactile information was recorded during the sliding motion of the robotic arm with a constant velocity. The obtained tactile data were entered into a neurorobotic texture classifier with a recurrent spiking neural network. To match the spiking activity of mechanoreceptor cells, the sensor data were encoded and then modeled. The resulting high-dimensional features were then continuously classified with a neurally implemented SVM. This proposed approach suffers high computational complexity as well.

The fast Fourier transform (FFT) was used in many studies to classify textures. The obtained tactile signals were transformed into the frequency domain to find the principal frequency of each material. Afterward, the computed fundamental frequencies were used to classify different textures. For instance, Hu *et al.* classified five different fabrics by sliding a finger-shaped sensor over their surfaces [36]. To classify cotton, linen, silk, and denim fabrics, Song *et al.* designed a mechanism to generate the relative motion at a certain speed between the PVDF film and the surface of the perceived fabric [37]. Another study employed a piezoelectric microphone. The obtained sound waves were segmented by FFT. A supervised learning vector quantization technique was then used to discriminate 18 materials [38]. An artificial finger equipped with a piezoelectric sensor was used to detect surface textures of different dimensions [39]. Tactile signals generated during the exploratory movement of the finger were converted to the frequency domain via FFT. Although many roboticists have used FFT to generate tactile features to identify different textures, the main limitations of this method is the need for the sliding time and velocity to be constant and known to classify materials with irregular or nonperiodic textures. The performance of the tactile object discrimination reviewed above is dependent on the tactile feature extraction and learning methods designed for particular experimental setup (such as specific tactile sensor technology, well-controlled tools, predefined exploratory movements). All have to be individually configured to perform efficiently.

B. Contribution

In contrast to the previous work, we propose a set of novel tactile descriptor which is robust regardless of the number of tactile sensors used in robotic systems (large-scale robotic skin), tactile sensor technology, exploration time, type of exploratory movements, and textural structure of objects and materials (periodic and nonperiodic texture).

We evaluated the performance of our proposed tactile descriptors with two different robotic platforms to discriminate among large numbers of objects or materials via their textural properties. Our contribution can be summarized as follows.

1) A robotic hand with multimodal robotic skin on the fingertips performed a set of active human-like exploratory movements, from simple sliding to complex exploratory movements to discriminate 120 materials and 30 hand-held objects from each other by means of their textural properties.

2) A humanoid robot equipped with a large artificial skin area classified 120 large objects with 120 surface textures and three different weights while the large objects were held by the hands, arms, and chest (upper body) of the robot during sliding.

II. Proposed Robust Tactile Descriptors

In earlier studies, researchers used different signal processing techniques for interpreting tactile signals. The Fourier transform in the frequency domain along with magnitude, skewness, and kurtosis in the time domain have been mostly employed to interpret vibro-tactile signals. The magnitude of the signal is highly sensitive to noise. Thus, it is necessary to design an appropriate filter or filter bank to remove interference from tactile signals, which is a computationally costly procedure.

The Fourier transform presents the relative power of each frequency and calculates frequency responses based on specific time. The Fourier tranform is therefore not suitable for analyzing nonstationary signals, particularly in the case of surface texture recognition in which the texture has nonuniform (irregular) properties. In this case, the Discrete Wavelet Transform (DWT) and short-time Fourier tranform may be the best techniques for analyzing nonstationary signals. They analyze a localized signal by windowing in the time/frequency domain. However, these methods deal with large data vectors (large feature vectors) causing difficulties at the classification phase. More features require more training samples, which results in an increase in computational complexity as well as the risk of overfitting.

To overcome these issues, we propose a set of fundamental tactile descriptor inspired by the Hjorth parameters [40], which were presented for real-time biological signal analyses (Electroencephalography/EEG). Our proposed tactile descriptors represent the statistical properties of the tactile signals in the time domains, *Activity*, *Mobility*, and *Complexity*.

The *Activity* (1) is the total power of a signal. The *Mobility* parameter (2) is the square root of the ratio of the variance of the first derivative of the signal to that of the signal. The *Complexity* (3) is the second derivative of the variance and shows how the shape of the signal is similar to a pure sine wave. If the signal is more similar to the sine wave, the complexity value converges to 1 as

$$\mathrm{Act}(\mathbf{S}) = \frac{1}{N}\sum_{n=1}^{N}(S_n - \bar{S})^2 \tag{1}$$

$$\mathrm{Mob}(\mathbf{S}) = \left(\frac{\mathrm{Act}(\frac{dS_n}{dn})}{\mathrm{Act}(\mathbf{S})}\right)^{-1/2} \tag{2}$$

$$\mathrm{Com}(\mathbf{S}) = \frac{\mathrm{Mob}(\frac{dS_n}{dn})}{\mathrm{Mob}(\mathbf{S})}. \tag{3}$$

In above-presented equations, $\mathbf{S}$ is a tactile data vector with N data samples ($n \in \{1, \ldots, N\}$) and $\bar{S} = \frac{1}{N}\sum_{n=1}^{N} S_n$ is the average value, or mean, of $\mathbf{S}$.

Tactile objects' exploration first requires an initiation of a static contact with the surface of objects by a hand or a sensitive skin area and then sliding the hand or body part/s (with sensitive skin) over the surface of objects (dynamic motion) [41], [42]. The transition from the static state to the dynamic state (and vice-versa) during tactile object exploration depends very much on the frictional properties of the surface texture of objects. Robotic systems (for instance, a robotic hand) need to apply more force to transit from the static state to the dynamic state in order to explore the surface of objects with a high friction coefficient. Such a transition affects the outer layer of the robotic skin (it is usually made of soft materials such as silicon). This results in deformation of the outer layer of the robotic skin, which generates linear or/and nonlinear correlation between outputs of tactile sensors in the soft skin.

In the previous work, tactile information recorded at the starting and the ending of objects' surface exploration were eliminated [26], [27], [29]. However, in our study, we exploit the entire tactile information perceived during the exploration procedure [43]. Therefore, we propose considering the linear correlation (4) and nonlinear correlation (5) between tactile signals/sensors as additional tactile features as

$$L^{\text{cor}}_{\mathbf{S},\mathbf{V}} = \frac{\sum_{n=1}^{N}(S_n-\bar{S}).(V_n-\bar{V})}{\sigma(\mathbf{S}).\sigma(\mathbf{V})} \tag{4}$$

$$N^{\text{cor}}_{\mathbf{S},\mathbf{V}} = 1-\frac{6\sum_{n=1}^{N}(R_k)^2_n}{N(N^2-1)}. \tag{5}$$

These features provide information about the frictional properties of the surface of objects with the robotic systems while exploring objects' textural properties. In the above-presented equations, $\mathbf{S}$ and $\mathbf{V}$ are vectors of data over time (input tactile signals) with N samples, and R_k is the difference between the rank of $\mathbf{S}$ and the rank of $\mathbf{V}$. (6)–(10) are shown at the bottom of this page.

$$\mathbf{D}^{b_1} = \left[\mathbf{A}^{b_1}_S;\mathbf{A}^{b_1}_V;\mathbf{M}^{b_1}_S;\mathbf{M}^{b_1}_V;\mathbf{C}^{b_1}_S;\mathbf{C}^{b_i}_V;\mathbf{L}^{b_1}_{S,V};\mathbf{N}^{b_1}_{S,V}\right] \tag{11}$$

$$\mathbf{D}^{1:b_N}_{\text{total}} = \left[\mathbf{D}^{b_1};\mathbf{D}^{b_2};\mathbf{D}^{b_3};\ldots;\mathbf{D}^{b_i};\ldots;\mathbf{D}^{b_{N-1}};\mathbf{D}^{b_N}\right]. \tag{12}$$

In (9) and (10), $\mathbf{L}^{b_i}_{S,V}$ and $\mathbf{N}^{b_i}_{S,V}$ are total linear and nonlinear correlations between the output of various tactile sensors/tactile signals, respectively. These parameters are averaged over each axis of the tactile sensors as well as entire skin modules ($n_c = 1,\ldots,N_c$) in each body part $b_i \in \mathcal{B}$. The proposed final feature descriptors for one body part of a robotic system or one limb of a humanoid robot ($b_i = b_1$) covered with a large number of multimodal tactile sensors $n_c = 1,\ldots,N_c$ with multiple axes $n_s = 1,\ldots,N_s$ can be defined as (11).

Equation (11) is the concatenation of total Activity, Mobility, Complexity parameters together with the total linear and nonlinear correlation coefficients as one feature vector with 24 data points. The proposed tactile descriptor for a robotic system or a humanoid, whose N body parts ($b_n = 1,\ldots,b_i,\ldots,b_N$) contributed in the tactile exploration with a large number of multimodal tactile sensors, can be written as (11). The tactile feature vector computed from N body parts ($\mathbf{D}^{1:b_N}_{\text{total}}$) includes $N \times 24$ data samples.

A. Proposed Tactile Descriptors for a Large Skin Area

In this study, we used our proposed fundamental parameters to construct a novel set of tactile descriptor to extract robust tactile information from a large number of tactile sensors

$$\mathbf{A}^{b_i}_S = \left[\frac{\lambda_{n_c}}{N_cN_s}\sum_{n_c=1}^{N_c}\sum_{n_s=1}^{N_s}\text{Act}(S^x_{n_c,n_s})^{b_i}, \frac{\lambda_{n_c}}{N_cN_s}\sum_{n_c=1}^{N_c}\sum_{n_s=1}^{N_s}\text{Act}(S^y_{n_c,n_s})^{b_i}, \frac{\lambda_{n_c}}{N_cN_s}\sum_{n_c=1}^{N_c}\sum_{n_s=1}^{N_s}\text{Act}(S^z_{n_c,n_s})^{b_i}\right] \tag{6}$$

$$\mathbf{M}^{b_i}_S = \left[\frac{\lambda_{n_c}}{N_cN_s}\sum_{n_c=1}^{N_c}\sum_{n_s=1}^{N_s}\text{Mob}(S^x_{n_c,n_s})^{b_i}, \frac{\lambda_{n_c}}{N_cN_s}\sum_{n_c=1}^{N_c}\sum_{n_s=1}^{N_s}\text{Mob}(S^y_{n_c,n_s})^{b_i}, \frac{\lambda_{n_c}}{N_cN_s}\sum_{n_c=1}^{N_c}\sum_{n_s=1}^{N_s}\text{Mob}(S^z_{n_c,n_s})^{b_i}\right] \tag{7}$$

$$\mathbf{C}^{b_i}_S = \left[\frac{\lambda_{n_c}}{N_cN_s}\sum_{n_c=1}^{N_c}\sum_{n_s=1}^{N_s}\text{Com}(S^x_{n_c,n_s})^{b_i}, \frac{\lambda_{n_c}}{N_cN_s}\sum_{n_c=1}^{N_c}\sum_{n_s=1}^{N_s}\text{Com}(S^y_{n_c,n_s})^{b_i}, \frac{\lambda_{n_c}}{N_cN_s}\sum_{n_c=1}^{N_c}\sum_{n_s=1}^{N_s}\text{Com}(S^z_{n_c,n_s})^{b_i}\right] \tag{8}$$

$$\mathbf{L}^{b_i}_{S,V} = \left[\frac{\lambda_{n_c}}{N_cN_sN_r}\sum_{n_c=1}^{N_c}\sum_{n_s=1}^{N_s}\sum_{n_r=1}^{N_r}L^{\text{cor}}(S^x_{n_c,n_s},V^x_{n_c,n_r})^{b_i}, \frac{\lambda_{n_c}}{N_cN_sN_r}\sum_{n_c=1}^{N_c}\sum_{n_s=1}^{N_s}\sum_{n_r=1}^{N_r}L^{\text{cor}}(S^y_{n_c,n_s},V^y_{n_c,n_r})^{b_i}, \frac{\lambda_{n_c}}{N_cN_sN_r}\sum_{n_c=1}^{N_c}\sum_{n_s=1}^{N_s}\sum_{n_r=1}^{N_r}L^{\text{cor}}(S^z_{n_c,n_s},V^z_{n_c,n_r})^{b_i}\right] \tag{9}$$

$$\mathbf{N}^{b_i}_{S,V} = \left[\frac{\lambda_{n_c}}{N_cN_sN_r}\sum_{n_c=1}^{N_c}\sum_{n_s=1}^{N_s}\sum_{n_r=1}^{N_r}N^{\text{cor}}(S^x_{n_c,n_s},V^x_{n_c,n_r})^{b_i}, \frac{\lambda_{n_c}}{N_cN_sN_r}\sum_{n_c=1}^{N_c}\sum_{n_s=1}^{N_s}\sum_{n_r=1}^{N_r}N^{\text{cor}}(S^y_{n_c,n_s},V^y_{n_c,n_r})^{b_i}, \frac{\lambda_{n_c}}{N_cN_sN_r}\sum_{n_c=1}^{N_c}\sum_{n_s=1}^{N_s}\sum_{n_r=1}^{N_r}N^{\text{cor}}(S^z_{n_c,n_s},V^z_{n_c,n_r})^{b_i}\right] \tag{10}$$

or a large robotic skin area. Our proposed feature descriptor includes the computed mean value of the Activity, Mobility, and Complexity of the tactile sensor's output over entire signal axes as well as tactile sensors/skin modules in one body part of the robotic system. In addition, our proposed descriptor includes the mean value of the linear and nonlinear correlation coefficients between tactile signals. More formally, suppose a body part/limb ($b_i \in \mathcal{B}$) of a robotic system/humanoid (for instance, a forearm or an upper arm of a humanoid) is covered with N_c skin cells/modules (one skin cell or skin module can have several tactile sensors with multiple sensing technologies). Each cell/module consists of N_s tactile sensors $(S_{n_c,n_s})^{b_i}$ with multiple axes, $(S^x_{n_c,n_s})^{b_i}$, $(S^y_{n_c,n_s})^{b_i}$, and $(S^z_{n_c,n_s})^{b_i}$ in which $n_c = 1, \ldots, N_c$, $n_s = 1, \ldots, N_s$, and $b_i \in \mathcal{B}$. More general, each skin cell/module includes multimodal tactile sensors $(S_{n_c,n_s})^{b_i}$, $(V_{n_c,n_r})^{b_i}$, $(U_{n_c,n_p})^{b_i}$, etc., where $n_c = 1, \ldots, N_c$, $n_r = 1, \ldots, N_r$, and $n_p = 1, \ldots, N_p$.

The total Activity, Mobility, and Complexity of a large number of multimodal tactile sensors or a large skin area over each body part ($b_i \in \mathcal{B}$) are described in (6), (7), and (8), respectively. Using the proposed descriptor (12), a robotic system or a humanoid robot can extract robust tactile information when exploring objects or surfaces with each body part or multiple body parts (even whole-body tactile exploration), as a human does.

Our proposed tactile descriptors are defined in the time domain and they can be interpreted in the frequency domain as well. The *Activity* (1) is the total power of a signal, which can also be interpreted as the surface of the power spectrum in the frequency domain (Parseval's relation). The *Mobility* parameter in (2) is the mean frequency estimation with a proportion of standard deviation of the power spectrum. The *Complexity* (3) as the second derivative of the power parameter estimates the bandwidth of the signal.

1) Built-in Tactile Sensor Selection: The contact may occur at any arbitrary location along with the skin of a robotic system with the surface of objects during the tactile object/surface exploration. Only those tactile sensors or skin modules that are in contact with the surface of the object need to be considered in the feature space. The key result of this inclusion is the decrease in computational cost and energy consumption. This is especially significant when a large number of tactile sensors or a large skin area are used. Our proposed feature descriptor contains a built-in tactile sensor or skin module selection λ_{n_c} in (6)–(10). By thresholding the force signals (13) to detect contact during tactile exploration, only those tactile sensors or skin cells/modules in parts of a body ($b_i \in \mathcal{B}$) interacting with the surface of the object will contribute in the feature vector as

$$\lambda_{n_c} = \begin{cases} 1 & \text{if } \frac{1}{N_r}\sum_{n_r=1}^{N_r} F_{n_c,n_r} \geq F_t \quad \text{Contact} \\ 0 & \text{Otherwise} \qquad\qquad\quad \text{No-contact} \end{cases}. \tag{13}$$

III. System Description

A. Robotic Skin

1) BioTac: BioTac is a multimodal electronic skin (see Fig. 1). When it moves over the surface of an object, the generated vibration can be measured by an embedded dynamic pressure sensor ($\mathbf{P}_{\mathrm{AC}}$) with the sampling data rate of 2.2 KHz. The BioTac has 19 impedance-sensing electrodes ($\mathbf{E}_1, \ldots, \mathbf{E}_{19}$) distributed over the surface of the rigid part [see Fig. 1(E)]. These electrodes are capable of measuring the deformation that arises when normal forces are applied to the surface of the skin with the sampling rate of 50 Hz. Moreover, the BioTac can measure low-frequency pressure ($\mathbf{P}_{\mathrm{DC}}$).

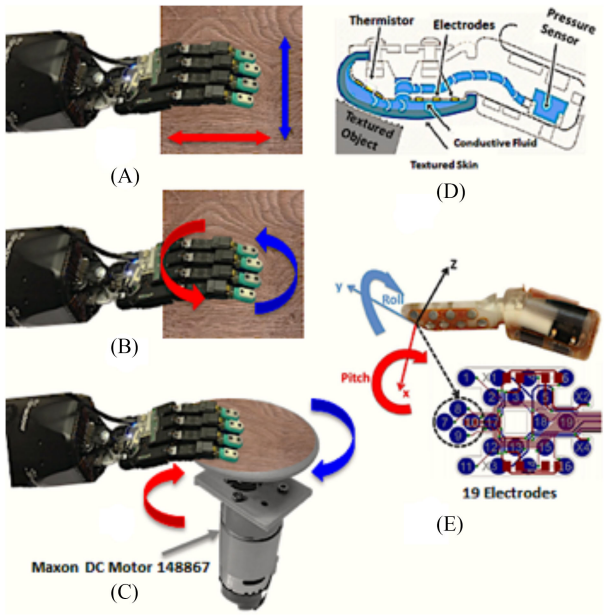

Fig. 1. Shadow Hand exploring the textural properties of materials. (A) shows the execution of the lateral and medial exploratory movements. (B) Shadow Hand performs a human-like circular exploratory motion. (C) Experimental material rotates underneath the fingertips of the Shadow hand with a constant velocity. (D) and (E) Demonstrate the BioTac sensors with their 19 impedance electrodes and one pressure sensor.

TABLE I
Cellular Skin Characteristics

Modality	Acceleration	Force	Proximity	Temperature
Sensor	BMA250	Customized	VCNL4010	LM71
Per Cell	1	3	1	1
Range	$\pm 2g$	$0-10N$	$1-200mm$	$-40-150°C$
Resolution	$10bit$	$12bit$	$16bit$	$14bit$
Bandwidth	$0-1kHz$	$0-33kHz$	$0-250Hz$	$0-7Hz$

2) Cellular Skin: In order to emulate a human sense of touch, we have designed and manufactured multimodal tactile sensors called *Cellular skin* [44] to provide robotic systems with the ability to sense the touch. Each skin cell has one microcontroller on the back and one set of multimodal tactile sensors on the front, including one *three-axis accelerometer*, one *proximity sensor*, three *normal-force sensors*, and one *temperature sensor* (see Table I). Skin cells are directly connected with each other via bendable and stretchable interconnectors. A unique cell ID is assigned to each skin cell within a network of skin patches to efficiently handle a large number of skin cells [see Fig. 2(B) and (C)].

B. Robotic Platform

1) Shadow Hand: The Shadow Hand is an advanced robotic hand system with five fingers equipped with the BioTac $f_i \in \mathcal{F} = \{$thumb, index finger, middle finger, ring finger, little

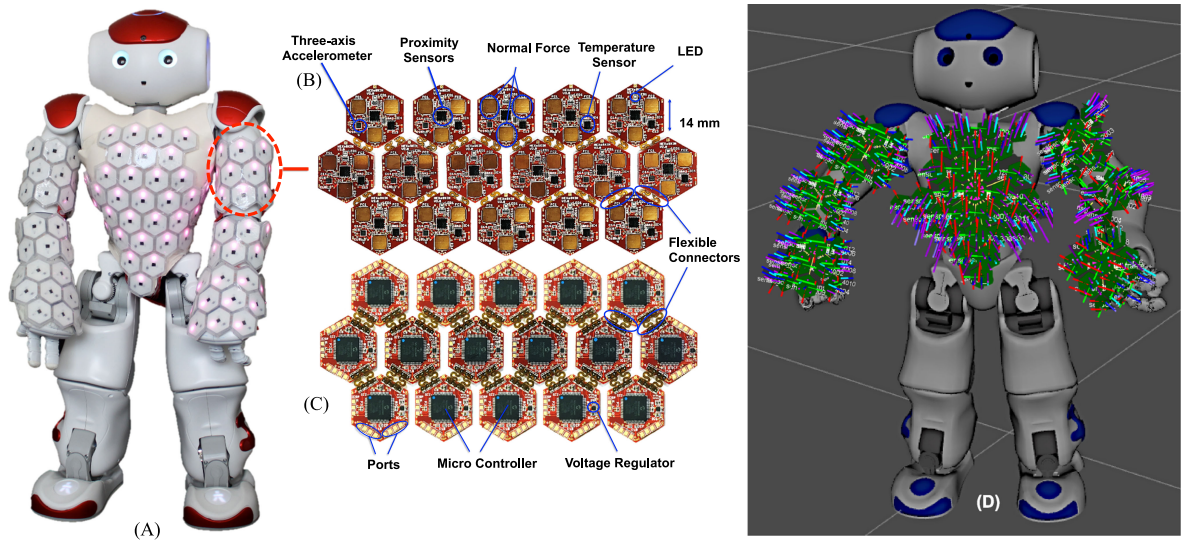

Fig. 2. (A) NAO is equipped with 116 multimodal artificial skin (Cellular skin) including 32 skin cells on the chest, and 14, 12, and 16 skin cells on each hand, fore arm, and upper arm, respectively. (B) and (C) Front and back of the Cellular skin. (D) Skin cells and NAO in rviz. We integrated skin cells with NAO via ROS.

finger}. It has 20 actuated +degree of freedom (DOF) and a further 4 underactuated movements for a total of 24 joints. Each joint has a movement range, that is the same as or very close to that of a human hand, including the thumb and even the flex of the palm for the little finger. The Shadow Hand is fully integrated with the BioTac through ROS (see Fig. 1).

2) NAO Humanoid Robot: NAO is a small humanoid with 25 DoF, a 1.6 GHz Intel Atom Central Processing Unit, and height and weight of 58 cm and 4.3 kg, respectively. We covered the upper body of the NAO with a thin layer of a flexible and stretchable material. In order to provide the humanoid with the sense of touch, we mounted 116 Cellular skin on the upper body of NAO: including 32 skin cells on the chest, and 14, 12, and 16 skin cells on each hand, forearm, and upper arm, respectively; see Fig. 2(A). In total, all seven body parts of NAO $b_i \in \mathcal{B} =$ {left hand, right hand, left forearm, right forearm, left upper arm, right upper arm, chest} were equipped with 348 *normal-force sensors*, 116 *three-axis accelerometer sensors*, 116 *proximity sensors*, and 116 *temperature sensors*. We fully integrated all skin cells with NAO via ROS [see Fig. 2(D)].

C. Tactile Descriptors for the Shadow Hand

While the Shadow Hand with the BioTac on the fingertips was executing sliding movements, the exploratory action generated two types of tactile data that were measured by the pressure sensor $\mathbf{P}_{\text{AC}}^{f_i}$ (with the sampling rate of 2.2 KHz) and the impedance sensing electrode array $\mathbf{E}_{n_r}^{f_i}$ (with the sampling rate of 50 Hz). In order to extract the robust tactile data, we assumed that the tactile information measured by $(\mathbf{P}_{\text{AC}}^{f_i})$ corresponded to high-frequency texture information and the tactile data sensed by $(\mathbf{E}_{n_r}^{f_i})$ related to the lower frequency changes in the texture, especially regarding nonuniform or transitional periods in the overall surface texture structure.

Our proposed feature descriptors were applied to the collected training and test dataset to extract robust tactile information. More formally, the robust tactile feature was computed by substituting each of the $(\mathbf{P}_{\text{AC}}^{f_i})$ and $(\mathbf{E}_{n_r}^{f_i})$ for $\mathbf{S}$ separately in (6), (7), and (8). Each finger of the Shadow Hand was considered as one body part $b_i = f_i \in \mathcal{F}\,(f_i = 1, 2, \ldots, 5)$ and one skin module $N_c = 1$. Each finger with one BioTac has one $(N_s = 1)$ single-axis $(\mathbf{P}_{\text{AC}}^{f_i})$ and $N_r = 19$ single-axis impedance electrodes $(\mathbf{E}_{n_r}^{f_i})$. The linear and nonlinear correlations between $(\mathbf{P}_{\text{AC}}^{f_i})$ and $(\mathbf{E}_{n_r}^{f_i})$ in each finger $(f_i \in \mathcal{F})$ were computed using (14) and (15). The total feature descriptor for one finger $(f_i \in \mathcal{F})$ includes $\mathbf{A}_{P_{\text{AC}}}^{f_i} = \lambda_{f_i}(\text{Act}(\mathbf{P}_{\text{AC}}^{f_i}))$, $\mathbf{M}_{P_{\text{AC}}}^{f_i} = \lambda_{f_i}(\text{Mob}(\mathbf{P}_{\text{AC}}^{f_i}))$, and $\mathbf{C}_{P_{\text{AC}}}^{f_i} = \lambda_{f_i}(\text{Com}(\mathbf{P}_{\text{AC}}^{f_i}))$, which are the computed mean value of the Activity, Mobility, and Complexity of the output of the dynamic pressure sensor $(\mathbf{P}_{AC}^{f_1})$, respectively, and $\mathbf{A}_E^{f_i} = \frac{\lambda_{f_i}}{N_r}\sum_{n_r=1}^{N_r}\text{Act}(E_{n_r}^{f_i})$, $\mathbf{A}_E^{f_i} = \frac{\lambda_{f_i}}{N_r}\sum_{n_r=1}^{N_r}\text{Mob}(E_{n_r}^{f_i})$, and $\mathbf{A}_E^{f_i} = \frac{\lambda_{f_i}}{N_r}\sum_{n_r=1}^{N_r}\text{Com}(E_{n_r}^{f_i})$, which are mean values of the Activity, Mobility, and Complexity of each impedance sensing electrode $(\mathbf{E}_{n_r}^{f_i})$. The mean value of the linear and nonlinear correlation coefficients between each impedance sensing electrode, and the dynamic pressure sensor were calculated with (14) and (15), respectively, as additional tactile features as

$$\mathbf{L}_{P_{\text{AC}},E}^{f_i} = \frac{\lambda_{f_i}}{N_r}\sum_{n_r=1}^{N_r} L^{\text{cor}}(\mathbf{P}_{\text{AC}},\, \mathbf{E}_{n_r}^{f_i}) \tag{14}$$

$$\mathbf{N}_{P_{\text{AC}},E}^{f_i} = \frac{\lambda_{f_i}}{N_r}\sum_{n_r=1}^{N_r} N^{\text{cor}}(\mathbf{P}_{\text{AC}},\, \mathbf{E}_{n_r}^{f_i}) \tag{15}$$

in which

$$\lambda_{f_i} = \begin{cases} 1 & \text{if} \quad \mathbf{P}_{\text{DC}}^{f_i} \geq 0.2\,N \quad \text{Contact} \\ 0 & \text{Otherwise} \quad\quad\; \text{No-Contact} \end{cases}. \tag{16}$$

$F_t = 0.2N$ in (16) is the minimum stable contact force that can be measured by the sensor and was determined during the experiments.

The final proposed feature descriptor for one finger $i = 1$ ($f_i \in \mathcal{F}$) is the concatenation of the total descriptors, which can be written as

$$\mathbf{D}^{f_1} = \left[A_{P_{\text{AC}}}^{f_1};\ A_E^{f_1};\ M_{P_{\text{AC}}}^{f_1};\ M_E^{f_1};\ C_{P_{\text{AC}}}^{f_1};\ C_E^{f_i};\ L_{P_{\text{AC}},E}^{f_1};\ N_{P_{\text{AC}},E}^{f_1}\right]. \tag{17}$$

The total tactile descriptors of five fingers contributed in the tactile object/surface exploration can be written as

$$\mathbf{D}_{\text{total}}^{\text{Shadow}} = \left[\mathbf{D}^{f_1};\ \mathbf{D}^{f_2};\ \mathbf{D}^{f_1};\ \mathbf{D}^{f_3} v\ \mathbf{D}^{f_4};\ \mathbf{D}^{f_5}\right]. \tag{18}$$

In the above-presented equations, $\mathbf{D}^{f_1}$ and $\mathbf{D}_{\text{total}}^{\text{Shadow}}$ include 8 and 8×5 data samples, respectively.

D. Tactile Descriptors for NAO

NAO perceived tactile signals related to textural properties of objects through their electronic skin. The tactile information corresponding to high-frequency texture information as well as low-frequency changes in the overall structure of the texture were measured by each three-axis accelerometer sensor ($\mathbf{a}_{n_c,n_s}$) and single-axis force sensors ($\mathbf{F}_{n_c,n_r}$) in each skin cell. The proposed tactile feature descriptors (6), (7), (8), (14), and (15) were used to extract the robust tactile information from the output of each axis of the accelerometer sensors (a_{n_c,n_s}^x, a_{n_c,n_s}^y, a_{n_c,n_s}^z) as well as force sensors ($\mathbf{F}_{n_c,n_r}$). The computed features were then averaged over the entire skin cells on each body part ($b_i \in \mathcal{B}$) of NAO. More formally, the Activity, Mobility, and Complexity of the accelerometers were computed by (19), (20), and (21), respectively. The robust tactile features were extracted from each of the force sensors by (22)–(24).

In this experiment, N_c is the number of the skin cells in one body part ($b_i \in \mathcal{B}$). $N_s = 1$ and $N_r = 3$ are the number of existing three-axis accelerometers and force sensors in one skin cell, respectively. In (27), $F_t = 0.2N$ is the minimum stable contact force.

The linear and nonlinear correlations between each axis of the accelerometer (a_{n_c,n_s}^x, a_{n_c,n_s}^y, a_{n_c,n_s}^z) and force sensors ($\mathbf{F}_{n_s,n_r}$) were calculated with (25) and (26), which were then averaged over all skin cells in a body part ($b_i \in \mathcal{B}$) as

$$\mathbf{A}_{\mathbf{a}}^{b_i} = \left[\frac{\lambda_{n_c}}{N_c}\sum_{n_c=1}^{N_c}\text{Act}(a_{n_c}^x)^{b_i},\ \frac{\lambda_{n_c}}{N_c}\sum_{n_c=1}^{N_c}\text{Act}(a_{n_c}^y)^{b_i},\ \frac{\lambda_{n_c}}{N_c}\sum_{n_c=1}^{N_c}\text{Act}(a_{n_c}^z)^{b_i}\right] \tag{19}$$

$$\mathbf{M}_{\mathbf{a}}^{b_i} = \left[\frac{\lambda_{n_c}}{N_c}\sum_{n_c=1}^{N_c}\text{Mob}(a_{n_c}^x)^{b_i},\ \frac{\lambda_{n_c}}{N_c}\sum_{n_c=1}^{N_c}\text{Mob}(a_{n_c}^y)^{b_i},\ \frac{\lambda_{n_c}}{N_c}\sum_{n_c=1}^{N_c}\text{Mob}(a_{n_c}^z)^{b_i}\right] \tag{20}$$

$$\mathbf{C}_{\mathbf{a}}^{b_i} = \left[\frac{\lambda_{n_c}}{N_c}\sum_{n_c=1}^{N_c}\text{Com}(a_{n_c}^x)^{b_i},\ \frac{\lambda_{n_c}}{N_c}\sum_{n_c=1}^{N_c}\text{Com}(a_{n_c}^y)^{b_i},\ \frac{\lambda_{n_c}}{N_c}\sum_{n_c=1}^{N_c}\text{Com}(a_{n_c}^z)^{b_i}\right] \tag{21}$$

$$\mathbf{A}_{\mathbf{F}}^{b_i} = \left[\frac{\lambda_{n_c}}{N_c N_s}\sum_{n_c=1}^{N_c}\sum_{n_r=1}^{N_r}\text{Act}(F_{n_c,n_r})^{b_i}\right] \tag{22}$$

$$\mathbf{M}_{\mathbf{F}}^{b_i} = \left[\frac{\lambda_{n_c}}{N_c N_r}\sum_{n_c=1}^{N_c}\sum_{n_r=1}^{N_r}\text{Mob}(F_{n_c,n_r})^{b_i}\right] \tag{23}$$

$$\mathbf{C}_{\mathbf{F}}^{b_i} = \left[\frac{\lambda_{n_c}}{N_c N_r}\sum_{n_c=1}^{N_c}\sum_{n_r=1}^{N_r}\text{Com}(F_{n_c,n_r})^{b_i}\right]. \tag{24}$$

(25)–(27) are shown at the bottom of this page. The final proposed feature descriptor for one body part of NAO ($b_i \in \mathcal{B}$) or the end-effecter of UR10 ($b_i = 1$) is the concatenation of the all descriptors, which can be written as

$$\mathbf{D}^{b_1} = \left[\mathbf{A}_{\mathbf{a}}^{b_1};\ \mathbf{A}_{\mathbf{F}}^{b_1};\ \mathbf{M}_{\mathbf{a}}^{b_1};\ \mathbf{M}_{\mathbf{F}}^{b_1};\ \mathbf{C}_{\mathbf{a}}^{b_1};\ \mathbf{C}_{\mathbf{F}}^{b_1};\ \mathbf{L}_{\mathbf{a},\mathbf{F}}^{b_1};\ \mathbf{N}_{\mathbf{a},\mathbf{F}}^{b_1}\right]. \tag{28}$$

The proposed tactile descriptors of upper body of NAO $b_i \in \mathcal{B} =$ {left hand, right hand, left forearm, right forearm, left upper

$$\mathbf{L}_{\mathbf{a},\mathbf{F}}^{b_i} = \left[\frac{\lambda_{n_c}}{N_c N_s N_r}\sum_{n_c=1}^{N_c}\sum_{n_s=1}^{N_s}\sum_{n_r=1}^{N_r}L^{\text{cor}}(a_{n_c,n_s}^x, F_{n_c,n_r})^{b_i},\ \frac{\lambda_{n_c}}{N_c N_s N_r}\sum_{n_c=1}^{N_c}\sum_{n_s=1}^{N_s}\sum_{n_r=1}^{N_r}L^{\text{cor}}(a_{n_c,n_s}^y, F_{n_c,n_r})^{b_i},\ \frac{\lambda_{n_c}}{N_c N_s N_r}\sum_{n_c=1}^{N_c}\sum_{n_s=1}^{N_s}\sum_{n_r=1}^{N_r}L^{\text{cor}}(a_{n_c,n_s}^z, F_{n_c,n_r})^{b_i}\right] \tag{25}$$

$$\mathbf{N}_{\mathbf{a},\mathbf{F}}^{b_i} = \left[\frac{\lambda_{n_c}}{N_c N_s N_r}\sum_{n_c=1}^{N_c}\sum_{n_s=1}^{N_s}\sum_{n_r=1}^{N_r}N^{\text{cor}}(a_{n_c,n_s}^x, F_{n_c,n_r})^{b_i},\ \frac{\lambda_{n_c}}{N_c N_s N_r}\sum_{n_c=1}^{N_c}\sum_{n_s=1}^{N_s}\sum_{n_r=1}^{N_r}N^{\text{cor}}(a_{n_c,n_s}^y, F_{n_c,n_r})^{b_i},\ \frac{\lambda_{n_c}}{N_c N_s N_r}\sum_{n_c=1}^{N_c}\sum_{n_s=1}^{N_s}\sum_{n_r=1}^{N_r}N^{\text{cor}}(a_{n_c,n_s}^z, F_{n_c,n_r})^{b_i}\right] \tag{26}$$

$$\lambda_{n_c} = \begin{cases} 1 & \text{if } \frac{1}{N_r}\sum_{n_r=1}^{N_r}F_{n_c,n_r} \geq 0.2\,N \quad \text{Contact} \\ 0 & O.W. \qquad\qquad\qquad\quad \text{No-Contact} \end{cases}. \tag{27}$$

Fig. 3. Selected experimental materials consist of 120 different natural and synthetic textures with uniform (regular) and nonuniform (irregular) structures including papers and vinyl wallpapers (Tex.#1-Tex.#37), textiles (Tex.#38-Tex.#57), carpets and mats (Tex.#58-Tex.#78), foams and sponges (Tex.#79-Tex.#82), fibers (Tex.#83,Tex.#84), PVC and rubber type surfaces (Tex.#85-Tex.#95), leathers and furs (Tex.#96-Tex.#100), wooden surfaces (Tex.#101-Tex.#109), metal surfaces (Tex.#110-Tex.#113), fiberglass and glass surfaces (Tex.#114-Tex.#118), and carbon sheets (Tex.#119,Tex.#120). All materials were acquired from Bauhaus.

arm, right upper arm, chest$\}$ contributed in the tactile texture exploration can be defined as

$$\mathbf{D}_{\text{total}}^{\text{NAO}} = \left[\mathbf{D}^{b_1};\, \mathbf{D}^{b_2};\, \mathbf{D}^{b_3};\, \mathbf{D}^{b_4};\, \mathbf{D}^{b_5};\, \mathbf{D}^{b_6};\, \mathbf{D}^{b_7}\right]. \quad (29)$$

In the above-presented equations, the feature vectors $\mathbf{D}^{b_1}$ and $\mathbf{D}_{\text{total}}^{\text{NAO}}$ include 18 and 7×18 data samples, respectively.

IV. Tactile Exploration With a Robotic Hand

Humans can discriminate among objects by means of their textural properties while sliding their fingertips on the surface of the objects. The exploratory behaviors can be either a simple lateral/medial sliding movement or a complex full hand circular motion in which the fingertips rotate to slid on the surface of the objects. Furthermore, we can discriminate among different hand-held objects by sliding our fingertips on their surfaces without consideration of their shape [45].

In this study, a set of active human-like exploratory movements, from simple sliding to complex exploratory movements, were carried out by the robotic hand to perceive the relevant tactile information about the textural properties of materials and objects (active exploration). Moreover, a rotational stage was designed to move experimental materials underneath the robotic hand to sense the corresponding tactile information of the materials (passive exploration).

A. Material Exploration With the Shadow Hand

1) Properties of Experimental Materials: The experimental materials consist of 120 various natural and synthetic surface textures with uniform and nonuniform textural structures (textures with different densities and sparsities). The difference in textural properties of experimental materials varied from relatively similar to quite different. The experimental materials include papers and vinyl wallpapers, textiles, carpets and mats, foams and sponges, fibers, PVC and rubber type surfaces, leathers and furs, wooden surfaces, metal surfaces, fiberglass and glass surfaces, and carbon sheets (see Fig. 3).

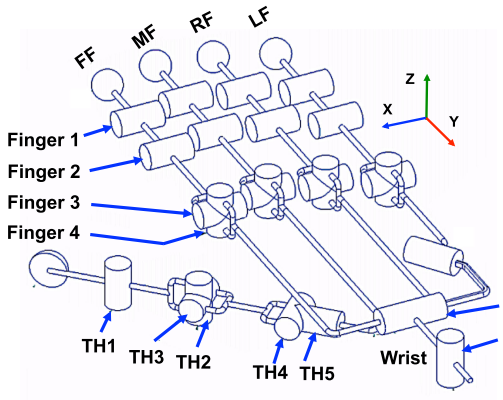

Fig. 4. Kinematics diagram of the Shadow Hand.

2) Lateral Sliding Exploratory Movement: The Shadow Hand with all five fingers open established a static contact [see Fig. 1(A)] with each of the experimental materials by moving its wrist toward their surfaces along the *Z*-axis (rotating the WR1 joint around the *X*-axis); see Fig. 3. Then, each finger was individually controlled to move around the *Z*-axis via the FF3, MF3, RF3, LF3, and TH4 joints (see Fig. 4) until each of them detected the minimum contact force $P_{\text{DC}}^{f_i} = 0.2N$ ($f_i \in \mathcal{F}$). The value of $P_{\text{DC}}^{f_i} = F_{\text{min}}^{f_i} = 0.2N$ is the minimum stable contact force that can be measured by the sensor and was determined during the experiments, in which we consider it as a "light contact of the Shadow Hand with a surface." The values of maximum force $F_{\text{max}}^{f_i} = 3N$ that was applied from each finger to the surface of the materials and maximum sliding velocity $v_{\text{max}} = 4$ cm/s were selected to avoid any damages to the tactile sensors as well as the robotic hand.

a) Training data collection: In order to collect training samples, the Shadow Hand executed a lateral sliding motion by moving its wrist from right to left and vice-versa for 4 cm (by rotating WR2 join around the *Z*-axis). The tactile signals perceived during the exploratory movements were measured

by dynamic pressure sensors $P_{\text{AC}}^{f_i}$ with a 2.2 KHz sampling rate and an impedance sensing electrode array $\mathbf{E}_{n_r}^{f_i}$ in which $n_r = 1, 2, \ldots, 19$ with a 50 Hz sampling rate (in total 100 tactile signals from the output of five BioTac sensors).

The applied force value for each finger f_i was chosen uniformly at random from $F^{f_i} \in \{F_{\text{min}}^{f_i}, F_{\text{min}}^{f_i} + \Delta f, F_{\text{min}}^{f_i} + 2\Delta f, \ldots, F_{\text{max}}^{f_i}\}$, in which $F_{\text{min}}^{f_i} = 0.2N$, $F_{\text{max}}^{f_i} = 3N$, and $\Delta f = 0.4N$. The applied force was then chosen for each finger f_i from $F^{f_i} \in \{0.2, 0.6, 1, 1.4, 1.7 \ldots, 3\}$. The velocity of the lateral sliding movement V (the velocity of hand or WR2 joint) was selected uniformly at random from $V_{\in}\{v_{\text{min}}, v_{\text{min}} + \Delta v_{\text{test}}, v_{\text{min}} + 2\Delta v, \ldots, v_{\text{max}}\}$, in which $v_{\text{min}} = 0.5$ cm/s, $v_{\text{max}} = 4$ cm/s, $\Delta v = 0.5$ cm/s, and $V \in \{0.5, 1, 1.5, 2, 2.5, \ldots, 4\}$. In order to ensure an unbiased and fair training data collection, the exploration time was considered to be fixed to $t = 2$ s. The selected applied force values for all fingers were kept constant during each exploration round by continuously measuring $P_{\text{DC}}^{f_i}$ ($f_i \in \mathcal{F}$) and controlling each finger via the FF3, MF3, RF3, LF3, and TH4 joints (see Fig. 4). The orientation of the experimental materials at each round varied by $\pi/4$ along the *Z*-axis. The exploratory action carried out each round once with each of 120 materials. The entire data collection procedure was repeated 20 times. At the end of each data collection round, the BioTac sensors were calibrated by measuring $P_{\text{DC}}^{f_i}$, $\mathbf{P}_{\text{AC}}^{f_i}$, and $\mathbf{E}_{n_r}^{f_i}$, and setting their outputs to zero when the sensors were not in contact with the materials.

b) Test data collection: To evaluate the performance of the proposed descriptor as well as the robot tactile learning, test data were collected separately. Contrary to the training part, the exploration time, at each round, was selected uniformly at random from $T_{\text{test}} \in \{t_{\text{min}}, t_{\text{min}} + \Delta t, t_{\text{min}} + 2\Delta t, \ldots, t_{\text{max}}\}$, in which $t_{\text{min}} = 2$ s, $t_{\text{max}} = 10$ s, $\Delta t = 1$ s, and $T_{\text{test}} \in \{2, 3, 4, \ldots, 10\}$. At each round, test data were collected with each of the 120 surfaces once. The orientation of the experimental materials varied by $\pi/6$ along the *Z*-axis. The entire test data collection was repeated 100 times. All data were collected over a time period of three weeks to take into account any changes in environmental conditions during the experiment.

3) Medial Sliding Exploratory Movement: The Shadow Hand with all fingers open initiated a static contact (light touch) with the surface of the experimental materials by rotating the WR1 joint around the *X*-axis (see Fig. 4). In order to perceive the tactile properties, the Shadow Hand slid all five fingers medially from up to down and vice-versa [see Fig. 1(A)] for 4 cm. The medial motion looked like the Shadow Hand closed and opened (and vice-versa) its fingers on the experimental surface.

a) Training data collection: In order to collect tactile data, the position and velocity of WR2, FF3, MF3, RF3, LF3, and TH3 joints (see Fig. 4) were controlled to generate the medial sliding movement. The exploratory motion parameters such as sliding velocity and applied force were selected from V and F^{f_i}, respectively. The exploration time at each round was $t = 2$ s. The rest of the data collection was identical to the training data collection procedure described for the lateral sliding movement.

b) Test data collection: The medial exploratory movement was performed by the Shadow Hand to collect the test data. The rest of the procedure was identical to the test data collection with the lateral sliding movement.

4) Circular Sliding Exploratory Movement: One of the most complex human hand exploratory motions is sliding of all five fingers circularly along the surface of an object. The aim of this part of the study was to examine the performance of our proposed descriptors by executing human-like complex exploratory motions. Since the hard coding of the Shadow Hand to generate such a motion was time consuming, we used the CyberGlove[1] (a data glove). The CyberGlove is fully integrated to the Shadow Hand via ROS. When a human subject wearing a CyberGlove moves fingers, the Shadow Hand can imitate the same movements. All kinematics values of the joints of the robotic hand while imitating the human hand motions, such as the position, orientation, and velocity of FF2, FF3, MF2, MF3, RF2, RF3, LF2, LF3, TH2 and TH3 joints, were recorded and then saved in a rosbag file. By playing back the rosbag files, the Shadow Hand could reproduce the same hand movements.

In this study, the exploratory motions of 11 human subjects, which consisted of 6 females and 5 males ranging from 20 to 40 years old, were captured. Each participant h_i was asked to wear the CyberGlove. Then, each subject established a static contact with the surface of a material and then moved his or her fingers circularly on the surface of the material for $T_{\text{max}} = 10$ s. At the same time, the Shadow Hand connected to the CyberGlove generated the same movements. The entire procedure was repeated 20 times with each subject and with a 15 min resting pause between each round. All recorded kinematics data were then added to a dataset $H \in \{h_1^{20}, h_2^{20}, \ldots, h_{11}^{20}\}$ in which h_i^{20} includes 20 separate rosbag files for subject h_i. It is noteworthy to mention that there was no tactile feedback available for the robot.

a) Training data collection: To collect training data, h_i^{20} was randomly selected from $H \in \{h_1^{20}, h_2^{20}, \ldots, h_{11}^{20}\}$. It is noteworthy to mentioned that in order to collect a fair training data and to evaluate our proposed descriptors systematically with the test data, the kinematics information (position, orientation, and velocity) of FF3, MF3, RF3, LF3, and TH4 in each rosbag were modified. However, this modification was less time consuming than hard coding of the robot to generate the human-like movements.

By playing back of each of the rosbag file h_i^{20}, the Shadow Hand regenerated human-like exploratory motion. The value of applied force for each finger f_i was selected individually from F^{f_i}. The selected applied force value F^{f_i} for each finger f_i was kept constant during each exploration. The rest of the procedure was the same as described for lateral and medial training data collection parts.

b) Test data collection: The Shadow Hand randomly selected ten exploratory motions from each of the ten remaining human subjects $H_{\text{test}} \in \{h_1^{10}, h_2^{10}, \ldots, h_{10}^{10}\}$. The robot reproduced 100 human-like circular exploratory movements to collect test data. The rest of test data collection remained identical to the previous test data collection parts.

5) Combined Exploratory Movement:

a) Training data collection: The combined exploratory movement was the combination of the three exploratory actions $lateral + medial + circular$. At each round, the Shadow

[1]http://www.cyberglovesystems.com/

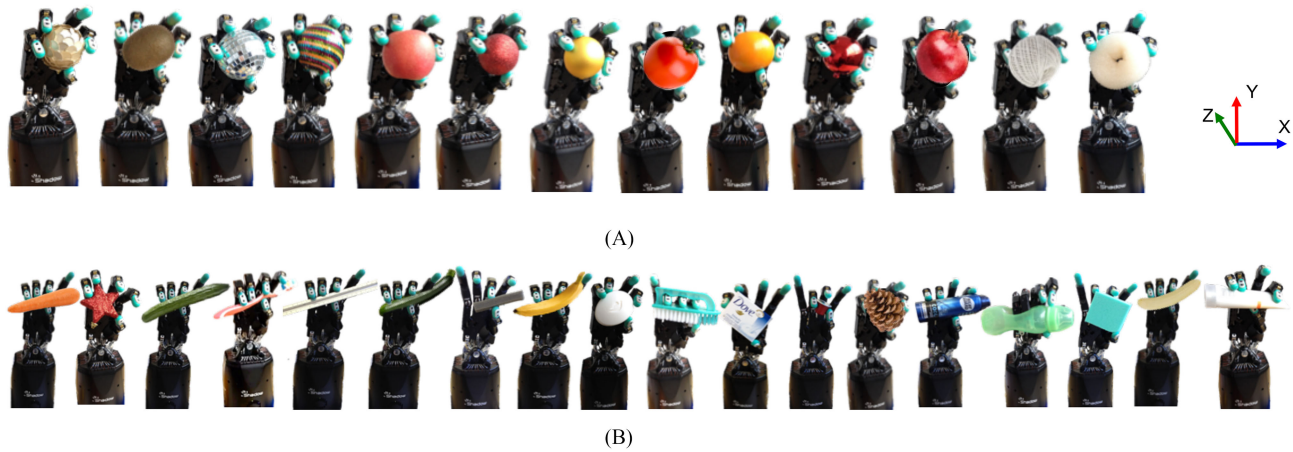

Fig. 5. (A) In-hand uniform shape objects. (B) In-hand complex shape objects.

Hand executed sequentially lateral, medial, and circular sliding movements ($S^{\text{comb}}_{\text{train}} = S_{\text{LMC}}$) on the surface of each material to collect tactile training data. The exploration time, at each round was $t = 3$ s. The rest of the procedure remained identical to the previous training data collection parts.

b) Test data collection: To collect test data, at each round, the exploratory action was uniformly selected at random from $S^{\text{comb}}_{\text{test}} \in \{S_L, S_M, S_C, S_{\text{LMC}}, S_{\text{LCM}}, S_{\text{MLC}}, S_{\text{MCL}}, S_{\text{CLM}}, S_{\text{CML}}\}$ and then was executed by the robot. The action set included the combination of lateral, medial, and circular motions with different sequences. For instance, S_{CML} means the Shadow Hand performed, in order, circular, medial, and lateral actions. The velocity of sliding and applied normal force were selected from V and F^{f_i}, respectively. The exploration time was chosen from T_{test} in which $t_{\text{min}} = 3$ s, $t_{\text{max}} = 10$ s, $\Delta t = 1$ s, and $T_{\text{test}} \in \{3, 4, 5, \ldots, 10\}$. The rest of the procedure was the same as the previous test data collection parts.

6) Rotational Stage: Previously, researchers have used well-controlled experimental devices to validate their proposed tactile descriptors. Therefore, to compare the performance of our proposed tactile feature extraction technique with the state-of-the-art, we have designed a well-controlled rotational stage Fig. 1(C). The system consists of a Maxon DC motor 148867 (GEARHEAD MAXON 203114, PLANETARY, 42MM, 4.3/1) and a 3-D printed plate made of poly lactic acid material with a radius of $r = 70$ mm. A Maxon motor control 145391 and an encoder HEDS5540 are used to control the velocity of the motor.

a) Training data collection: Each experimental material was attached firmly to one 3-D printed plate. The velocity of the motor was kept constant with a frequency of $f^M = 0.1011$ Hz during training data collection. The Shadow Hand established a light contact with the experimental surface $P^{f_i}_{\text{DC}} = 0.2N$. The same applied force values for all fingers were selected from F^{f_i}. The attached material was rotated underneath of all five fingertips for $t = 2$ s. The rest of the procedure was identical to the previous training data collection parts.

b) Test data collection: In order to collect test data similar to the previous studies, the velocity of the motor and the applied force value were deliberately chosen to be the same as in the training part.

B. In-Hand Object Exploration With the Shadow Hand

1) Properties of In-Hand Objects: In this study, 32 natural and synthetic everyday objects with uniform (regular) and nonuniform (irregular) textural properties were selected. Fourteen objects with an identical geometrical shape (in this case a spherical shape) were chosen, including a tomato, apple, pomegranate, kiwi, orange, a pine cone textured ball with an irregular texture, a mirror texture ball, two plastic balls with an almost similar smooth surface texture, a rough textured ball, a colorful ball with a smooth surface, a rough spherical sponge, and a string ball with an irregular texture [see Fig. 5(A)]. Additionally, 18 objects with different complex shapes including a banana, zucchini, carrot, cucumber, a peeled banana, pine cone, a toothbrush, a floor brush, a soap, a memory sponge, a cardboard box, a rough textured star, a coffee capsule, a spray bottle, and a plastic baby feeder [see Fig. 5(B)]. In both sets of objects, the difference in the surface texture properties varied from relatively similar to quite different. Humans can discriminate among in-hand objects by perceiving their textural properties whilst sliding their fingertips on the surfaces regardless of the object's shape.

2) Training Data Collection: Each experimental object was placed between the thumb (TH), little (LF), and ring (RF) fingers of the robot (see Fig. 4). Then, the Shadow Hand started closing its fingers to hold the object. The tactile feedbacks from $P^{\text{LF}}_{\text{DC}}$, $P^{\text{RF}}_{\text{DC}}$, and $P^{\text{TH}}_{\text{DC}}$ was utilized to refine the current pose of the object and stabilize the current grasp. The grasp force values of each experimental object (with different stiffness and friction coefficients) were determined individually during the experiment. The grasp force was kept constant during each exploration by continuously measuring the outputs of $P^{\text{LF}}_{\text{DC}}$, $P^{\text{RF}}_{\text{DC}}$, $P^{\text{TH}}_{\text{DC}}$ and by controlling the position of the (LF2, LF3), (RF2, RF3), and (TH2,TH3,TH4,TH5) joints. However, this can be done autonomously by the robot by implementing a slip detection and deformation prevention method. We will consider this improvement as a future work by implementing our recently proposed slip detection and deformation prevention strategy in to the Shadow Hand [21].

In order to perceive the textural properties of each in-hand object, the robot used its index (FF) and middle (MF) fingers to establish a light contact with the surface of each object

$P_{\text{DC}}^{\text{FF}} = 0.2N$ and $P_{\text{DC}}^{\text{MF}} = 0.2N$. Afterward, the Shadow Hand slid each index and middle finger 2 cm on the surface of the in-hand object by rotating FF2 and MF2 around the *X*-axis. Tactile data were measured by the BioTac sensors using the impedance electrodes ($\mathbf{E}_{n_r}^{\text{FF}}$ and $\mathbf{E}_{n_r}^{\text{MF}}$) and the pressure sensors ($P_{\text{AC}}^{\text{FF}}$ and $P_{\text{AC}}^{\text{MF}}$), in total 40 tactile signals from the output of two BioTac sensors. The maximum applied force ($F_{\text{max}}^{f_i} = 2N$) as well as the maximum sliding velocity $v_{\text{max}} = 4$ cm/s were selected to avoid any damage to the in-hand objects. The selected sliding velocity V and the applied normal force F^{f_i} at each round were kept identical in both fingers. In this case, $V \in \{v_{\text{min}}, v_{\text{min}} + \Delta v, v_{\text{min}} + 2\Delta v, \ldots, v_{\text{max}}\}$, $F^{f_i} \in \{F_{\text{min}}^{f_i}, F_{\text{min}}^{f_i} + \Delta f, F_{\text{min}}^{f_i} + 2\Delta f, \ldots, F_{\text{max}}^{f_i}\}$. In which $v_{\text{min}} = 0.5$ cm/s, $v_{\text{max}} = 4$ cm/s, $\Delta v = 0.5$ cm/s, $F_{\text{min}}^{f_i} = 0.2N$, $F_{\text{max}}^{f_i} = 2N$, $\Delta f = 0.4N$ ($V \in \{0.5, 1, 1.5, \ldots, 4\}$, and $F^{f_i} \in \{0.2, 0.6, 1, \ldots, 2\}$). At each round, the training data were collected once with each of the experimental object. The entire data collection repeated 20 times. At each round, the experimental objects were held with $\pi/4$ perturbation in the pose around the *X*-axis. At the end of each round, the BioTac sensors were calibrated.

3) Test Data Collection: The robotic hand used its little, ring, and middle fingers to grasp each object. Afterward, the robot with its thumb and index established light contact with the surface of the hand-held object ($P_{\text{DC}}^{\text{FF}} = 0.2N$ and $P_{\text{DC}}^{\text{MF}} = 0.2N$). Then, the robot slid its thumb and index 1 cm on the surface of the object by rotating (TH3, TH4) and FF2 joints around the *X*-axis. The selected velocity of the sliding movement and the value of the applied force for the thumb and index finger were chosen separately from V, F^{f_i}. At each exploration round, the velocity and applied force values were kept constant by measuring $P_{\text{DC}}^{\text{TH}}$ and $P_{\text{DC}}^{\text{FF}}$ and controlling the position of the TH3 and Th4 joints for the thumb and FF2 and FF3 for the index finger. The exploration time was chosen from $T_{\text{test}} \in \{t_{\text{min}}, t_{\text{min}} + \Delta t, t_{\text{min}} + 2\Delta t, \ldots, t_{\text{max}}\}$ in which $t_{\text{min}} = 2$ s, $t_{\text{max}} = 10$s, and $T_{\text{test}} \in \{2, 3, \ldots, 10\}$. At each round, test data were collected once with each of the 32 experimental in-hand objects. The orientation of the hand-held objects varied by $\pi/4$ around the *X*-axis. The entire test data collection was repeated 100 times.

V. Tactile Exploration With a Humanoid

Humans can sense the textural properties of objects by sliding a sensitive body part with large skin area (such as the hand, lower arm, upper arm, etc.) on the surface of the objects. In order to grasp and lift an unknown large object, we utilize both our hands and arms and even the upper part of our body, such as our chest. In this case, a large area of our skin is in contact with the surface of the large object. As the large object starts sliding between our hands and arms, we can recognize the physical properties of the large object. In this part of the study, a set of active human-like exploratory movement was executed by NAO having large-scale artificial skin to perceive the textural properties of 120 materials and 120 large objects with different weights W_i. In addition, a rotational stage was used to move the experimental materials underneath the NAO's hand.

A. Material Surface Exploration With NAO

1) Lateral Sliding Exploratory Movement: NAO initiated a static contact with the surface of the material by moving either its right hand via the RShoulderPitch joint or the left hand using the LShoulderPitch joint until the average of the total normal force sensors on the hand reached $\frac{1}{N_r N c} \sum_{n_c=1}^{N_c} \sum_{n_r=1}^{N_r} F_{n_c,n_r} = 0.2N$ (light contact), in which $N_r = 3$ is the number of the normal force sensor in each skin cell and $N_c = 14$ is the number of the skin cell mounted on one hand. Afterward, NAO explored the textural properties of the materials by sliding its hand laterally "$d\ cm$" on the surface of the material by moving the RShoulderRoll or LShoulderRoll joint (see Fig. 6). Tactile information was measured by the force sensors F_{n_c,n_r} with a 250 Hz sampling rate and three-axis accelerometer sensors $\mathbf{a}_{n_c,n_s}$ with a 1 KHz sampling rate, in which $n_s = 1, 2, 3$ ($N_s = 3$) is the number of the axis of the accelerometer (in total 84 tactile signals from the output of 14 skin cells on the hand). The maximum force that NAO applied with its hand to the surface of the materials was $F_{\text{max}}^{\text{hand}} = \frac{1}{N_r N c} \sum_{n_c=1}^{N_c} \sum_{n_r=1}^{N_r} F_{n_c,n_r} = 3N$ and the maximum velocity of the sliding was $v_{\text{max}} = 4$ cm/s.

a) Training data collection: In order to collect training samples, NAO slid its right hand 2 cm on the surface of each 120 materials once, which was then repeated 20 times. The velocity of the sliding movement and the value of the applied force were chosen from $V \in \{v_{\text{min}}, (v_{\text{min}} + \Delta v), (v_{\text{min}} + 2\Delta v), \ldots, v_{\text{max}}\}$, $F^{\text{hand}} \in \{F_{\text{min}}^{\text{hand}}, (F_{\text{min}}^{\text{hand}} + \Delta f_{\text{test}}), (F_{\text{min}}^{\text{hand}} + 2\Delta f), X, F_{\text{max}}^{\text{hand}}\}$, respectively, in which $v_{\text{min}} = 0.5$ cm/s, $\Delta v = 0.5$ cm/s, $F_{\text{min}}^{\text{hand}} = 0.2N$, $\Delta f = 0.4N$. For instance $V \in \{0.5, 1, 1.5, 2, \ldots, 4\}$ and $F^{\text{hand}} \in \{0.2, 0.6, 1, 1.4 \ldots, 3\}$. The values of $\Delta f = 0.4N$ and $\Delta v = 0.5$ s were determined based on the sensitivity and stability of the skin cells and NAO's hardware constrain.

The exploration time at each round was $t = 2$ s. The orientation of the experimental materials, at each round, varied by $\pi/4$ around the *Z*-axis. At the end of each exploration, each skin cell was calibrated by measuring the outputs of the sensors F_{n_c,n_r}, $\mathbf{a}_{n_c,n_s}$ and removing their biased signals (offset) when the skin cells were not in contact with the materials.

b) Test data collection: Humanoid robots should be able to recognize the textural properties of the objects with both the left and right hand, even though only one of them was used during the training phase. Here, NAO collected test data by sliding its left hand 1 cm on the surface of the materials. The exploration time, at each round, was chosen from T_{test} with $t_{\text{min}} = 2$ s, $t_{\text{max}} = 10$ s, $\Delta t = 1$. At each round, the orientation of the experimental materials varied by $\pi/6$ around the *Z*-axis. The entire data collection procedure was repeated 100 times. The rest of the procedure was the same as in the training data collection.

2) Medial Exploratory Sliding Movement: In order to generate the medial exploratory movement, NAO moved its hand forward and backward (along the *Y*-axis). NAO executed the medial movement with its right hand to collect training data by controlling the positions and velocities of the RShoulderPitch, RElbowRoll, and RElbowYaw joints in order to slide its hand 2 cm on the surface of the materials. The test data were

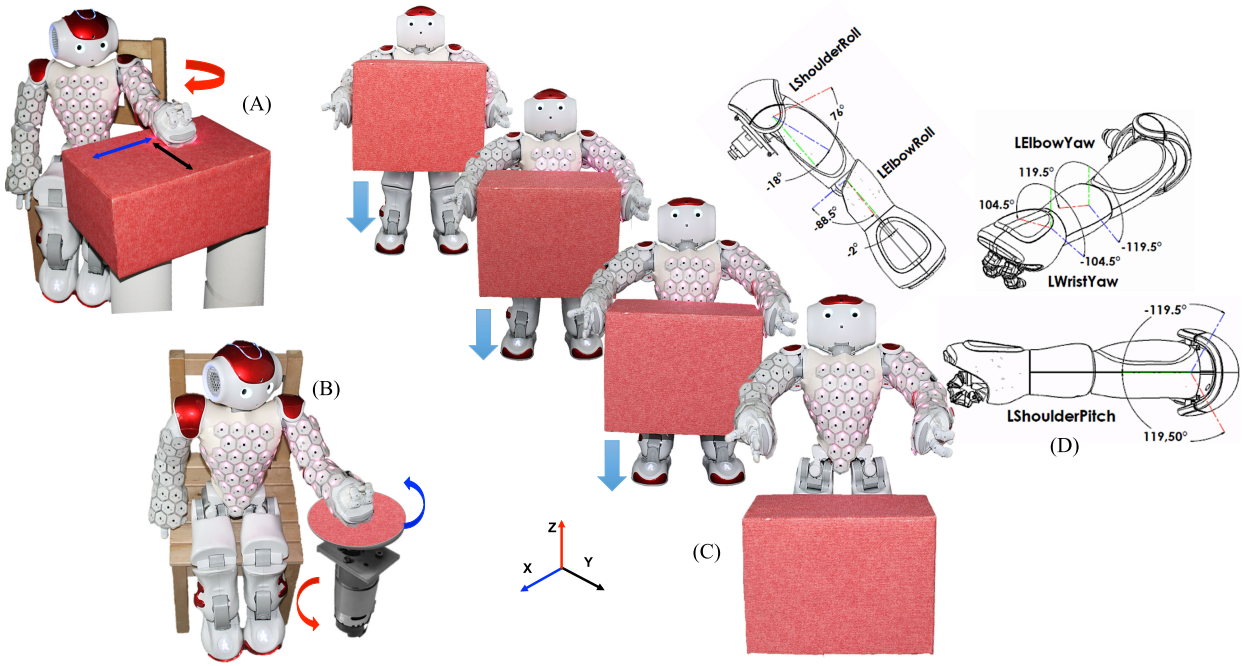

Fig. 6. (A) NAO executes lateral, medial, or circular exploratory movements to sense the textural properties of the object (active exploration). (B) Experimental material/texture rotates underneath of NAO's hand with a constant velocity (passive exploration). (C) Large object was held by NAO with its upper body slides gradually between its hands, arms, and chest (passive exploration).

collected with the left hand using the LShoulderPitch, LElbowRoll, and LElbowYaw joints while sliding 1 cm on the materials' surfaces (see Fig. 6). The rest of the training and test data collection procedure remained the same as described above.

3) Circular Sliding Exploratory Movement: NAO explored the textural properties of the materials and collected training data by sliding its right hand circularly (clockwise) on the materials' surfaces. The robot was programmed to move its hand circularly by controlling the positions and velocities of the RShoulderRoll, LShoulderPitch, RElbowRoll, and RElbowYaw (see Fig. 6). To collect test data, the circular motion was generated with the left hand (counter clockwise) via the LShoulderRoll, LShoulderPitch, LElbowRoll, and LElbowYaw joints. The rest of the training and test data collection process remained the same as explained in previous parts.

4) Combined Exploratory Movements: All three exploratory movements were combined as one motion (lateral + medial + circular). In this case, at each round, NAO continuously slid its hand laterally, medially, and circularly to explore the textural properties of each object. The data collection procedures remained identical to the previous parts. However, the exploration time in the training data collection phase at each round was $t = 6$ s and, for the test data collection was, selected from T_{test}, in which $t_{\text{min}} = 3$ s, $t_{\text{max}} = 15$ s, $\Delta t = 3$ s or $T_{\text{test}} \in \{3, 6, 9, 12, 15\}$.

a) Training data collection: The combined exploratory movement was performed with the right hand of NAO to collect training data. At each round, NAO sequentially performed the lateral, medial, and circular sliding movements ($S_{\text{train}}^{\text{comb}} = S_{\text{LMC}}$) on the surface of each material for $t = 3$s. The rest of the procedure remained identical to the previous training data collection parts.

b) Test data collection: The test data were collected with the NAO's left hand. The exploratory action was uniformly selected at random from $S_{\text{test}}^{\text{comb}} \in \{S_L, S_M, S_C, S_{\text{LMC}}, S_{\text{LCM}}, S_{\text{MLC}}, S_{\text{MCL}}, S_{\text{CLM}}, S_{\text{CML}}\}$. The exploration time was selected from T_{test}, in which $t_{\text{min}} = 3$ s, $t_{\text{max}} = 10$ s, $\Delta t = 1$ s, and $T_{\text{test}} \in \{3, 4, 5, \ldots, 10\}$. The rest of the procedure was the same as the previous test data collection parts.

5) Rotational Stage: In this part of the experiment, the same experimental setup, as in Section IV-A6, was used to collect tactile data by NAO's hands [see Fig. 6(B)]. The rest of the experiment remained identical to the training and test data collection explained earlier.

B. Large Object Exploration With NAO

1) Properties of the Large Objects: Taking into account NAO's size and weight, we created 360 large objects with the same dimension $32 \times 22 \times 14$ cm^3 (see Fig. 6) and three different weight categories: 120 objects weighing 500 g, 120 objects weighing 1000 g, and 120 objects weighing 1500 g. We then covered the surface of each set of objects with 120 different surface textures (see Fig. 3).

a) Training data collection: In this scenario, NAO was standing at the front of a table. Both its arms were straight and parallel to each other and it was able to open and close them in the horizontal direction (X-axis) using the LShoulderRoll and RShoulderRoll joints. The experimental object was placed between NAO's arms. Afterward, NAO slowly closed its arms to

grasp the object. However, the position of the object between NAO's arm could vary slightly along the arms or the *Y*-axis [see Fig. 6(C)]. To be sure that all 14 skin cells on each hand were in contact with the surface of the object during the grasp, NAO used the feedback from proximity sensors ($\mathbf{P}_{n_c}$). Proximity sensors give a measurement of the closeness corresponding to each skin cell with an experimental object's surface (which is called precontact or pretouch). If a skin cell is close to the surface of an object ($d_{n_c} < 3$ cm), in which d_{n_c} is the distance of one cell n_c from the surface, the normalized output of the proximity sensor is equal to one $\mathbf{P}_{n_c} = 1$, otherwise $\mathbf{P}_{n_c} = 0$. As soon as NAO realized its hands were close enough to the surface of the object via proximity ($d_{n_c} < 3$ cm), it moved its arms n steps ($n = 1, \ldots, 5$ and at each step 0.5 cm) forward or backward along the *Y*-axis using the LShoulderRoll, LElbowRoll, and LElbowYaw joints of the left hand and RShoulderRoll, RElbowRoll, and RElbowYaw joints of the right hand until it was sure that all skin cells on each hand would be in contact with the surface of the object. Afterward, it started closing its arms to grasp the object. As soon as the average of the total force sensors on the hand exceeded the grasping force value $\frac{1}{N_r N_c}\sum_{n_c=1}^{N_c}\sum_{n_r=1}^{N_r} F_{n_c,n_r} > f_{o_i}^{\text{grasp}}$, it lifted the large object 10 cm from the table using the LShoulderPitch and RShoulderPitch joints. The value of the force to grasp an object firmly $f_{o_i}^{\text{grasp}}$ within NAO's arm was determined during the experiments based on the objects' weights, as we did not implement any slip detection and deformation prevention methods on NAO ($f_{500}^{\text{grasp}} = \frac{1}{N_r N_c}\sum_{n_c=1}^{N_c}\sum_{n_r=1}^{N_r} F_{n_c,n_r} = 2N$, $f_{1000}^{\text{grasp}} = 2.7N$, and $f_{1500}^{\text{grasp}} = 3.5N$). Afterward, NAO pulled the large object (o_i) toward its chest by moving its arms backward along the *Y*-axis until the large object was in contact with its chest and NAO detected $\frac{1}{N_r N_c}\sum_{n_c=1}^{N_c}\sum_{n_r=1}^{N_r} F_{n_c,n_r} = 0.2N$ via the skin cells of the chest ($N_c = 32$ skin cells). As the experiment proceeded, NAO slowly opened its arms until the object started to slide between its arms and chest. When the object slid, it generated vibrations on the large skin area. The caused vibro-tactile signals were measured by accelerometers ($\mathbf{a}_{n_c,n_s}$) and force sensors ($\mathbf{F}_{n_c,n_r}$) on the hands, fore arms, upper arms, and chest (in total, 696 tactile signals from 116 skin cells). At each round, the exploration was carried out once with each of the 120 objects weighing 1000 g, which was repeated 20 times.

It is noteworthy to mention that in this experiment, the exploration time (sliding time), velocity of sliding, and value of applied normal force were dependent on the large objects' weights. In other words, objects with different weights slide with different velocities. Moreover, the robot needs to apply different force values by its hand to the surface of the object in order to grasp and then lift them up.

b) Test data collection: The test data collection were carried out as described for training data collection [see Fig. 6(C)]. However, the test exploration was repeated 100 times; 50 times for each large object weighing 500 g and 50 times for objects weighing 1500 g and 120 different surface textures. The exploration or sliding time, velocity of sliding, and the amount of applied force were different from the training data collection part as they varied depending on the objects' weights.

VI. Robot Learning Methodologies

To evaluate the performance and robustness of our proposed tactile descriptors across different learning algorithms, a range of commonly used learning techniques were applied, including an online or open-ended learning algorithm, a batch supervised learning method, as well as an unsupervised learning technique.

A. Passive Aggressive (PA) Online Learning

The robotic systems employed the cost-sensitive multiclass PA method to discriminate among M classes of objects or materials while receiving samples continuously over time. The PA is a margin-based online or open-ended learning technique in order to construct and update learning models continuously [46]. Using PA, at each time step, the robot constructed texture models to generate the corresponding prediction for the current received samples. The received true label was then used as feedback in order to update the texture models for the next new samples.

More formally, PA estimates the model parameters $\mathbf{w}_t \in \mathbb{R}^d$ at time $t = 1, 2, \ldots, T$ receives new data samples $\{\mathbf{x}_m, y_m\}_{m=1}^{M}$ where $\mathbf{x}_m \in \mathbb{X} \subset \mathbb{R}^n$ are sequential samples with $y_m \in \mathbb{Y}$ as their corresponding labels. Assume that the PA is provided with a set of d features $\phi_1, \ldots, \phi_d$ where each feature ϕ_i is a mapping from $\mathbb{X} \times \mathbb{Y}$ to the reals. We denote by $\Phi(\mathbf{x_m}, y_m) = (\phi_1(x_m, y_m), \ldots, \phi_d(x_m, y_m))$ the vector formed by concatenating the outputs of the features. At $t = 1$, the PA starts with the model parameters having values equal to zero. It means at $t = 1$, $\mathbf{w}_1 = (0, \ldots, 0)$, then the value of confidence in prediction was computed with $\hat{y}_t = \arg\max_{\mathbf{y}\in\mathbb{Y}}(\mathbf{w}_t \cdot \Phi(\mathbf{x}_{m,t}, y_{m,t}))$. Afterward, PA updates the models when it receives new samples by solving

$$\mathbf{w}_{t+1} = \min_{\mathbf{w}\in\mathbf{R}^d} \frac{1}{2}\|\mathbf{w} - \mathbf{w}_t\|^2 + \eta\xi \tag{30}$$

which results in

$$\mathbf{w}_{t+1} = \mathbf{w}_t + \theta_t(\Phi(\mathbf{x}_{m,t}, y_{m,t}) - \Phi(\mathbf{x}_{m,t}, \hat{y}_{m,t})) \tag{31}$$

$$\theta_t = \min \left\{ \eta, \frac{\max\{0, 1 + \mathbf{w}_t \cdot (\Phi(\mathbf{x}_{m,t}, y_{m,t}) - \Phi(\mathbf{x}_{m,t}, \hat{y}_{m,t}))}{\|\Phi(\mathbf{x}_{m,t}, y_{m,t}) - \Phi(\mathbf{x}_{m,t}, \hat{y}_{m,t})\|^2} \right\}. \tag{32}$$

In (30), η is a positive value that governs the influence of the slack terms. This technique is known as a PA-I cost sensitive multiclass classification with a prediction-based update (PB) [46]. ξ is a nonnegative scaling factor of the objective cost function. In (31), $\mathbf{x}_{m,t}$ is a current received sample at time t and $\mathbf{y}_{m,t}$ is the label of the received samples.

B. Support Vector Machine (SVM)

The SMV [47] was used to construct tactile object classification models from the extracted tactile features received during the training phase. While providing labeled training data (supervised learning), the algorithm constructs a hyperplane or a set of hyperplanes in a high-dimensional space in order to classify new objects from their textural properties.

C. Expectation Maximization (EM)

The EM algorithm [48] for Gaussian Mixture Models (GMM) with a spherical covariance matrix was employed to categorize objects via their textures. Given a GMM, the goal is to maximize the likelihood function with respect to the parameters (comprising the means and covariances of the components and the mixing coefficients). EM is an unsupervised and iterative algorithm that generalizes *k*-means to a probabilistic setting in four steps.

a) *Evaluating the output of clustering:* The normalized mutual information (NMI) method [49] was used to measure the quality of the clustering results. To do this, let $A = \{a_1, \ldots, a_K\}$ and $B = \{b_1, \ldots, a_S\}$ be two different partitions of the N data points, i.e., two different clusterings. For instance, A might be the estimated clustering (predicted labels) and B is the reference clustering derived from the class labels (true labels). Let's assume $p_{AB}(i,j) = |a_i \cap b_j|/N$ is the probability that a randomly selected object belongs to cluster a_i in A and b_i in B. Moreover, let $p_A(i) = |a_i|/N$ be the probability that a randomly selected object belongs to cluster a_i in A. Similarly, let's us define $p_A(i) = |a_i|/N$ for object b_i in B. The mutual information between cluster A and B can be written as

$$\mathbb{I}(A,B) = \sum_{i=1}^{K}\sum_{j=1}^{S} p_{AB}(i,j)\,\log\frac{p_{AB}(i,j)}{p_A(i)p_B(j)}. \tag{33}$$

$\mathbb{I}(A,B)$ lies between 0 and $\min\{H(A), H(B)\}$ in which $H(A)$ and $H(B)$ are entropy of A and B, respectively. The NMI is defined as

$$\text{NMI}(A,B) = \frac{I(A,B)}{(H(A)+H(B))/2}. \tag{34}$$

$\text{NMI}(A,B) \in [0,1]$, $\text{NMI}(A,B) = 0$ means no mutual information and $\text{NMI}(A,B) = 1$ means perfect correlation.

VII. Experimental Results

A. Experimental Results With the Shadow Hand

1) Supervised Material Discrimination: An SVM classifier [47] with a linear kernel was employed by the robotic hand to discriminate among materials/objects via their textural properties. To obtain the best learning parameters and the regularizer value C, fivefold cross validation (CV) was carried out on the entire training dataset. In this regard, the collected training set was randomly split into five folds; four of those for training and one for evaluation. The procedure was repeated ten times to obtain an average performance on the evaluation sets. The entire process was repeated 20 times with different values for $C \in \{10^{-4}, 5^{-4}, 3^{-4}, 2^{-4}, \ldots, 2^4, 3^4, 5^4, 10^4\}$ to find the one with the lowest CV error. Afterward, the SVM with the optimal parameters was retrained with the entire training set to construct the learning models, which were then used by the Shadow Hand for the prediction of the unseen, separately collected test set.

If a robot uses its full hand to learn about the textural properties of materials, it should be able to discriminate among materials (during the evaluation phase) with each of its finger or different combinations of two, three, four, or five fingers.

TABLE II
Surface Textures Classification by Shadow Hand

Exploratory Behavior	Training with	Test with	SVM
Lateral sliding	Full Hand (five fingers)	Combination of different number of fingers (from one finger to five fingers)	100%
Medial sliding			100%
Circular sliding			100%
Combination of Lateral, Medial, and Circular			100%
Rotational sliding			100%

The best regularizer value that was found by CV for all experiments is C = 0.001.

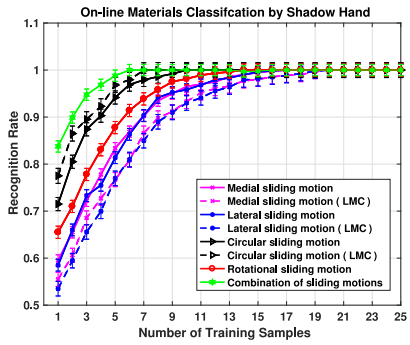

Fig. 7. Results of online material classification by the Shadow Hand.

In this experiment, the SVM was trained with the training data collected with all five fingers (full hand) of the Shadow Hand to construct learning texture models. To evaluate the robustness of our proposed tactile descriptors, the constructed tactile learning models were evaluated to predict with the test data $S_{\text{test}}^{1:100} \in \{S_f^1, S_f^2, \ldots, S_f^{100}\}$, in which f was uniformly selected at random from $f \in \{f_{\text{FF}}, f_{\text{MF}}, \ldots, (f_{\text{FF}}\ f_{\text{MF}}), (f_{\text{MF}}\ f_{\text{RF}}), \ldots, (f_{\text{FF}}\ f_{\text{MF}} f_{\text{RF}}), \ldots, (f_{\text{FF}}\ f_{\text{MF}} f_{RF}\ f_{\text{LF}}\ f_{\text{TH}})\}$. For instance, $S^1_{(f_{\text{FF}} f_{\text{MF}})}$ includes only the contribution of the index finger and middle finger during text data collection. Table II shows that the robotic hand successfully discriminated among 120 materials with a 100% recognition rate when it performed each of five exploratory motions while sliding with different combination of its fingers.

2) Online Material Discrimination: There is a tradeoff between the complexity of learning algorithms and the power of tactile descriptors in the tactile object and material discrimination domains. Using state-of-the-art feature extraction techniques, the robotic systems needed to store a large number of samples (as a batch of data) in its memory during training. The growth of object classes results in a memory explosion, making the state-of-the-art feature descriptors unfit for real-time robotic systems. In this experiment, we investigated whether it is possible for the robots to discriminate materials and objects with an online learning algorithm (low memory consumption) while utilizing our proposed descriptors.

To evaluate this, the Shadow Hand employed the PA algorithm to classify 120 experimental materials online. Using our proposed descriptors, the robotic hand constructed texture models while receiving training samples sequentially and over time ($t = 1, \ldots, 20$). In this experiment, the learning parameter η was fixed to 1. The recognition rates at each time t were computed by using the currently constructed learning models to predict test data. Fig. 7 shows the averaged classification rate at each training step ($t = 1, \ldots, 20$) with the lateral, medial, circular, and rotational exploratory behaviors. Fig. 7 illustrates that the

Shadow Hand achieved 100% recognition accuracy after training with 15 samples with each of the exploratory movements. Fig. 7 demonstrates that the Shadow Hand with circular sliding exploratory movements and ten training samples ($t = 10$) obtained 100% classification accuracy. Furthermore, we evaluated the performance of tactile material discrimination with the combination of all test datasets $S^{1:100}_{\text{LMC}_{\text{test}}} \in \{S^{1:100}_{L_{\text{test}}}, S^{1:100}_{M_{\text{test}}}, S^{1:100}_{C_{\text{test}}}\}$. To do this, we combined all test data collected by executing the lateral ($S^{1:100}_{L_{\text{test}}}$), medial ($S^{1:100}_{M_{\text{test}}}$), and circular ($S^{1:100}_{C_{\text{test}}}$) sliding actions (300 samples in total). Afterward, 100 samples were selected uniformly at random from the combined dataset $S^{1:100}_{\text{LMC}_{\text{test}}} \in \{S^{1:100}_{L_{\text{test}}}, S^{1:100}_{M_{\text{test}}}, S^{1:100}_{C_{\text{test}}}\}$. The constructed texture models then were evaluated to predict test samples in $S^{1:100}_{\text{LMC}_{\text{test}}}$. Fig. 7 shows that the Shadow Hand obtained 96% discrimination accuracy with 15 trials with the lateral and medial exploratory actions, which is slightly lower than when it was evaluated with the test data collected either with lateral ($S^{1:100}_{L_{\text{test}}}$) or medial ($S^{1:100}_{M_{\text{test}}}$) sliding movement. Moreover, Fig. 7 illustrates that the robotic hand successfully achieved 100% classification accuracy with seven training samples with circular sliding motion. This is due to the fact that some of the experimental materials, such as carpets and textiles, have multidirectional textures. In this case, the circular sliding motion provided rich tactile information in all directions (X-Y direction). In other words, the circular exploratory action helped the robot to learn about the textural properties of the materials with a few samples and more quickly than when it explores the materials with either a medial or lateral sliding motion. However, the robotic system receiving a few more training samples achieved the same recognition performance as obtained with the circular sliding motion.

In another experiment, the PA algorithm sequentially received 20 training samples that were obtained by the robot while performing the combined exploratory action ($S^{\text{comb}}_{\text{train}} = S_{\text{LMC}}$) on the surface of the materials. The constructed texture models at each time t were evaluated to predict the test data collected with different combinations of the exploratory actions $S^{\text{comb}}_{\text{test}} \in \{S_L, S_M, S_C, S_{\text{LMC}}, S_{\text{LCM}}, S_{\text{MLC}}, S_{\text{MCL}}, S_{\text{CLM}}, S_{\text{CML}}\}$. The combination of lateral, medial, and circular motions as one motion ($S^{\text{comb}}_{\text{train}}$ provided the richest tactile information with the robotic hand). In this case, the Shadow Hand achieved 100% classification accuracy with only six training samples. Let us consider the circular exploratory movement as the combination of the lateral and medial movements. Then, the combined exploratory motion is actually the combination of two lateral movements and two medial movements. Therefore, upon each movement, it provides more tactile information with the robotic hand at each exploration.

3) Supervised In-Hand Object Discrimination: This experiment scrutinized whether tactile in-hand object recognition performance depends only on how well and robustly the robotic hand could interpret the perceived tactile surface texture information of the held objects regardless of their shapes. The Shadow Hand should be able to discriminate in-hand objects via their textural properties without considering the geometrical properties of the in-hand objects (proprioceptive information) while moving its fingers slightly on the surface of in-hand objects. To evaluate this capability, the Shadow Hand used the SVM with the linear kernel method. To construct the tactile learning models, the SVM with the optimal learning parameters was trained by tactile features generated from the collected training set with uniform shape objects [see Fig. 5(A)]. The constructed tactile models were then evaluated to predict the corresponding test set. The learning procedure was repeated with training and test sets of the complex shape objects [see Fig. 5(B)]. Table III also shows that the Shadow Hand classified in-hand objects with uniform shapes from each other via their texture properties with 98.5% recognition accuracy. Moreover, it discriminated in-hand complex shape objects with 98.7% recognition accuracy.

TABLE III
IN-HAND OBJECTS CLASSIFICATION WITH SVM BY THE SHADOW HAND

In-Hand Objects	Training with	Test with	SVM
Identical Shape Objects	Index finger	Thumb	98.5%
Complex Shape Objects	&	&	98.7%
Mixed Shape Objects	Middle finger	Index finger	98.3%

The best regularizer value that was found by CV for all experiments is $C = 0.003$.

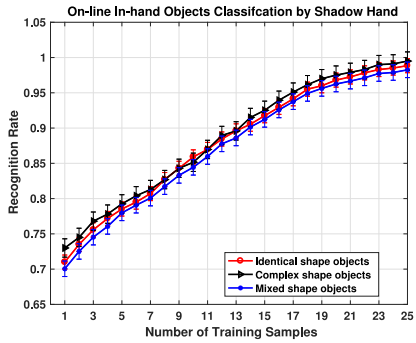

Fig. 8. Results of online in-hand objects classification by the Shadow Hand.

Furthermore, an additional experiment was carried out. The Shadow Hand was trained with the combined training sets of uniform and complex shape objects. Using constructed tactile object models, the robot successfully distinguished 30 multiple shaped in-hand objects from each other with 98.3% recognition accuracy. Table III also shows that the Shadow Hand successfully classified in-hand objects with multiple shapes via their textural properties (cutaneous information) regardless of their shapes (proprioceptive information) similar to humans.

4) Online In-Hand Objects Discrimination: In this experiment, the Shadow Hand used the online PA algorithm.

The same learning procedures, as described before, was performed with each of the trial samples of identical shape, complex shape, and multiple shape in-hand objects separately. The constructed texture models at each time step ($t = 1, \ldots, 20$) were evaluated using entire corresponding test stets. Fig. 8 shows the classification accuracy rate corresponding to *Identical Shape Objects*, *Complex Shape Objects*, and *Multiple Shape Objects*. The experimental outcomes (see Fig. 8) show that the Shadow Hand successfully recognized identical, complex, and multiple shape objects via their surface textures with a high

TABLE IV
RESULTS OF MATERIAL AND IN-HAND OBJECT CATEGORIZATION BY THE SHADOW HAND

Exploratory Behavior	NMI
Lateral sliding motion	0.92
Medial sliding motion	0.91
Circular sliding motion	0.92
Combination of Lateral, Medial, and Circular sliding motions	0.95
Rotational sliding	0.93
In-hand Identical Shape Objects	0.87
In-hand Complex Shape Objects	0.84
In-hand Mixed Shape Objects	0.85

TABLE V
SURFACE TEXTURES CLASSIFICATION BY NAO

Exploratory Behavior	Training with	Test with	SVM
Lateral sliding	Right Hand	Left Hand	97.1%
Medial sliding			97.3%
Circular sliding			98.2%
Combination of Lateral, Medial, and Circular			98.5%
Rotational sliding			97.9%

The best regularizer value that was found by CV for all experiments is $C = 0.005$.

average recognition rate that is substantially better than chance. The robotic hand achieved an average recognition rate of 96% with only 20 training samples online. Fig. 8 illustrates that the Shadow Hand, when receiving a few samples in sequence ($t = 21, \ldots, 25$), could have achieved 100% recognition rate.

5) Unsupervised Materials and In-Hand Objects Categorization: In this experiment, the robotic systems employed the EM algorithm as an unsupervised learning approach to categorize materials/objects via their textural properties. In this way, the EM was trained with the entire unsupervised dataset in all scenarios. The EM algorithm was initialized by the k-means clustering. The number of cluster k was set to be equal to the number of classes of the experimental materials or objects. The k-means algorithm was repeated 20 times each time and the EM algorithm iterated 100 times. The NMI was used to evaluate the clustering results. Table IV illustrates that the Shadow Hand successfully categorized among the experimental materials and clustered the in-hand objects via their textural properties in all schemes. The discrimination performance of an in-hand objects in all scenarios is a bit lower than the performance of materials classification. The reduction in accuracy for in-hand object discrimination is due to the variations in the contact positions that occurred during exploration, as there was no active slip detection and prevention method implemented in the robotic hand.

B. Experimental Results With NAO

1) Supervised Material Discrimination: NAO used the SVM to classify 120 materials via their textural properties. In order to construct learning models, the SVM with the optimal learning parameters was trained with the training data (collected with the right hand). The constructed learning models then were evaluated to predict the test data (collected with the left hand). Table V illustrates that NAO classified 120 materials with higher than 97% accuracy in all schemes.

2) Supervised Large Object Discrimination: The main goal of this experiment was to evaluate the performance of the proposed tactile descriptor while extracting tactile features from a large number of tactile sensors (a large skin area). The other goal was to investigate whether the discrimination of objects along surface texture properties is independent of an object's weight during passive exploration. The velocity of an object sliding between NAO's arms and chest relates directly to the object's weight; any variation in the object's weight should not affect the texture perception. In other words, NAO should recognize large objects sliding between its arms and chest (passive exploration) via their textural properties and regardless of their weights.

TABLE VI
LARGE OBJECTS DISCRIMINATION WITH SVM BY NAO

Large Objects	Training with	Test with	SVM
Large Objects with 500 g weight	Upper Body (large skin area)	Upper Body (large skin area)	90.6%
Large Objects with 1000 g weight			90.9%
Large Objects with 1500 g weight			91%
Large Objects with Mixed weight			90.5%

The best regularizer value that was found by CV for all experiments is $C = 0.003$.

In this regard, SVM was trained with a training set collected with objects with the same 1000 g weight and 120 various surface textures. The constructed texture models were examined using test sets including objects with 500 and 1500 g weights. Table VI illustrates that NAO successfully classified large objects with 90.6% recognition accuracy.

In order to assess the efficiency of the proposed tactile descriptors across various objects' weights, the experiment was repeated with different training and test sets. In this regard, NAO was trained with a training set of the large objects with 500 g and then examined using test sets including objects with 1000 and 1500 g and 120 different textures. The same procedure was performed with training sets of objects of 1500 g and test sets of objects of 500 and 1000 g. The final experiment in this context was conducted with a training set of objects of 500, 1000, and 1500 g, and the robot learning system was evaluated using an unseen test set separately collected with objects of 500, 1000, and 1500 g.

Table VI demonstrates the classification performance in which NAO discriminated 120 large objects through their surface properties regardless of any variation in objects' weights during the experiment. Objects with various weights but the same surface texture properties tend to be recognized as the same class of object. The reduction in discrimination performance is due to some variation with the position of the large object during sliding between the robot's arms and chest.

3) Online Material Discrimination: NAO used the PA algorithm in order to learn about the textural properties of 120 materials online. The same learning procedure, as described before, was performed with the training and test data. Fig. 9 displays that NAO obtained higher than 93% recognition with each of the exploratory movements with only 20 training samples. Moreover, NAO with circular exploratory movement and ten training samples ($t = 10$) obtained 90% classification accuracy.

Furthermore, the performance of the material exploration with each of the lateral, medial, and circular sliding movements was separately evaluated with the combination of all test data ($S^{1:100}_{\mathrm{LMC}_{\mathrm{test}}}$). Fig. 9 illustrates that NAO achieved 93%

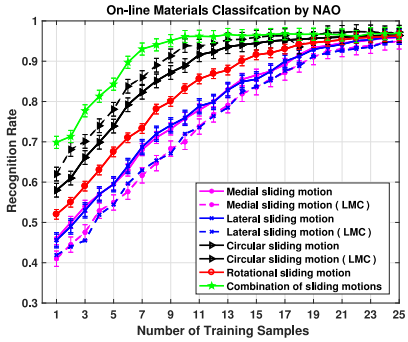

Fig. 9. Results of online material texture classification by NAO.

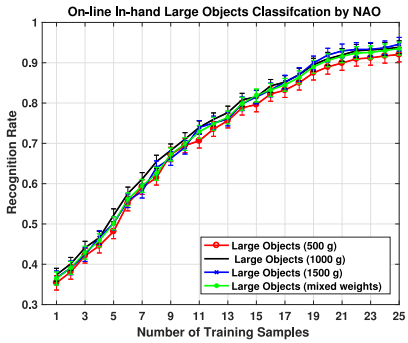

Fig. 10. Results of online large objects classification by NAO.

classification accuracy with 24 training samples using either lateral or medial exploratory action. In this scenario, the humanoid obtained a 90% recognition rate with only nine training samples. Fig. 9 also displays that NAO obtained a 95% recognition rate when it received ten trials with the combined exploratory movement ($S_{\text{train}}^{\text{comb}} = S_{\text{LMC}}$). In this case, at each time t the constructed texture models were evaluated to predict the test data collected with different combinations of the exploratory actions $S_{\text{test}}^{\text{comb}} \in \{S_L, S_M, S_C, S_{\text{LMC}}, S_{\text{LCM}}, S_{\text{MLC}}, S_{\text{MCL}}, S_{\text{CLM}}, S_{\text{CML}}\}$.

4) Online Large Object Discrimination: Fig. 10 shows that NAO successfully discriminated large objects using its large-scale skin with very high recognition rates online. The obtained classification performance is comparable with the performance NAO achieved with the SVM (batch learning). However, using the online learning method, the robot consumed much less memory to store data. This is due to the power of our proposed tactile descriptors that provided the robot with rich tactile information.

C. Materials and Large Objects Categorization

The EM algorithm as an unsupervised learning approach was used to categorize materials and large objects via their textural properties. The same procedure, as described before, was performed with the entire unsupervised data collected by NAO. Table VII illustrates that the NAO successfully clustered all 120 experimental materials and also 120 large objects via their textural properties in all schemes.

TABLE VII
RESULTS OF MATERIALS CATEGORIZATION BY NAO

Exploratory Behavior	NMI
Lateral sliding motion	0.88
Medial sliding motion	0.89
Circular sliding motion	0.91
Combination of Lateral, Medial, and Circular motions	0.93
Rotational sliding	0.92
In-hand Large Objects (500g)	0.81
In-hand Large Objects (100g)	0.83
In-hand Large Objects (1500g)	0.85
In-hand Large Objects (Mixed weights)	0.87

VIII. DISCUSSION

In order to evaluate the performance of our proposed tactile descriptors, we conducted an extensive experiment with multiple robotic systems, various tactile sensing technologies, and large number of natural and synthetic objects and materials. In this regard, the Shadow Hand and NAO with artificial skin successfully classified 120 various materials with regular and irregular structures while executing active human-like exploratory movements. The experiment was extended to the scenario of in-hand object discrimination, in which the robotic hand discriminated 30 uniform- and complex-shaped objects with regular and irregular textural properties. Moreover, the robustness and computational efficiency of the proposed descriptors were assessed with a humanoid with a large sensing area. The achieved high recognition rate by NAO shows that our tactile descriptors provided robust tactile information from the large number of tactile signals for discriminating among large objects via their surface texture regardless of their weight.

The experimental results show that the Shadow Hand obtained higher tactile discrimination accuracy than NAO in all scenarios. This is due to the fact that the BioTac has high spatial resolution, and the existing ridges on its outer layer help to better sense the textural properties of the objects/materials.

We further evaluated the robustness of our tactile descriptors using our proposed probabilistic active tactile learning method [50] and the active target object search algorithm [51]. Following our proposed methods, an industrial robotic arm (UR10) with the multimodal tactile sensors on the end-effector and also an industrial three-finger gripper (Robotiq) with the sense of touch on fingertips (OptoForce sensors) autonomously and efficiently discriminated natural objects via their textural properties. Furthermore, taking advantage of our proposed tactile descriptors, we developed the active tactile transfer learning methods to enable the robotics systems to reuse their constructed prior textural models while learning about new set of objects with a few training samples or even one [52]–[54].

IX. CONCLUSION

In this study, we proposed a set of robust tactile descriptors for a robotic system with artificial skin to discriminate among objects and materials by means of their textural properties. The performance of the proposed feature descriptors was evaluated with a large number of materials and in-hand objects, as well as large objects with periodic and nonperiodic surface texture. Moreover, we assessed the robustness of our tactile descriptors with multiple robotic systems that had a large multimodal

artificial skin area and various tactile sensing technologies, such as dynamic pressure sensors, accelerometers, capacitive sensors, and impedance electrode arrays. Using the proposed tactile descriptors while executing human-like exploratory movements, the Shadow Hand classified 120 materials (100% accuracy) and 30 in-hand objects (98% accuracy) via their textural properties. NAO with its upper body covered with multimodal tactile sensors identified 120 large objects with 90% accuracy, regardless of their weight.

REFERENCES

[1] R. S. Johansson and J. R. Flanagan, "Coding and use of tactile signals from the fingertips in object manipulation tasks," *Nature Rev. Neurosci.*, vol. 10, pp. 345–359, 2009.

[2] G. Robles-De-La-Torre, "The importance of the sense of touch in virtual and real environments," *IEEE MultiMedia*, vol. 13, no. 3, pp. 24–30, Jul. 2006.

[3] M. Kaboli, A. Long, and G. Cheng, "Humanoids learn touch modalities identification via multi-modal robotic skin and robust tactile descriptors," *Adv. Robot.*, vol. 29, no. 21, pp. 1411–1425, 2015.

[4] R. S. Dahiya, G. Metta, M. Valle, and G. Sandini, "Tactile sensing—from humans to humanoids," *IEEE Trans. Robot.*, vol. 26, no. 1, pp. 1–20, Feb. 2010.

[5] M. Kaltenbrunner *et al.*, "An ultra-lightweight design for imperceptible plastic electronics," *Nature*, vol. 499, pp. 455–463, 2013.

[6] M. W. Strohmayr, H. Worn, and G. Hirzinger, "The DLR artificial skin parti: Uniting sensitivity and robustness," in *Proc. IEEE Int. Conf. Robot. Autom.*, 2013, pp. 1012–1018.

[7] M. Kaboli, K. Yao, and G. Cheng, "A modular, distributed, soft, 3-axis sensor system for robot hands," in *Proc. IEEE Int. Conf. Humanoid Robots*, 2016, pp. 752–757.

[8] A. Schmitz, P. Maiolinoand, M. Maggiali, L. Natale, G. Cannata, and G. Metta, "Methods and technologies for the implementation of large-scale robot tactile sensors," *IEEE Trans. Robot.*, vol. 27, no. 3, pp. 389–400, Jun. 2011.

[9] J. Ulmen and M. Cutkosky, "A robust, low-cost and low-noise artificial skin for human-friendly robots," in *Proc. IEEE Int. Conf. Robot. Autom.*, 2010, pp. 4836–4841.

[10] Y. Ohmura, Y. Kuniyosh, and A. Nagakubo, "Conformable and scalable tactile sensor skin for curved surfaces," in *Proc. IEEE Int. Conf. Robot. Autom.*, 2006, pp. 1348–1353.

[11] H. Xie *et al.*, "Fiber optics tactile array probe for tissue palpation during minimally invasive surgery," in *Proc. IEEE Int. Conf. Intell. Robots Syst.*, 2013, pp. 2539–2544.

[12] R. S. Dahiya *et al.*, "Piezoelectric oxide semiconductor field effect transistor touch sensing devices," *Appl. Phys. Lett.*, vol. 95, 2009, Art. no. 034105.

[13] T. V. Papakostas, J. Lima, and M. Lowe, "A large area force sensor for smart skin applications," in *Proc. IEEE Sens.*, 2002, vol. 5, pp. 1620–1624.

[14] D. Hughes and N. Correll, "Texture ecognition and localization in amorphous robotic skin," *Bioinspiration Biomimetics*, vol. 10, 2015, Art. no. 055002.

[15] S. Denei, P. Maiolino, E. Baglini, and G. Cannata, "On the development of a tactile sensor for fabric manipulation and classification for industrial applications," in *Proc. IEEE Int. Conf. Intell. Robots Syst.*, 2015, pp. 5081–5086.

[16] N. Yogeswaran *et al.*, "New materials and advances in making electronic skin for interactive robots," *Adv. Robot.*, vol. 29, no. 21, pp. 1359–1373, 2015.

[17] S. Lee *et al.*, "A transparent bending-insensitive pressure sensor," *Nature Nanotechnol.*, vol. 11, pp. 472–478, 2016.

[18] H. Liu, J. Greco, X. Song, J. Bimbo, and K. Althoefer, "Tactile image based contact shape recognition using neural network," in *Proc. IEEE Int. Conf. Multisensor Fusion Int. Intell. Syst.*, 2013, pp. 138–143.

[19] M. V. Liarokapis, B. Calli, A. J. Spiers, and A. M. Dollar, "Unplanned, model-free, single grasp object classification with underactuated hands and force sensors," in *Proc. IEEE Int. Conf. Intell. Robots Syst.*, 2015, pp. 5073–5080.

[20] K. Yao, M. Kaboli, and G. Cheng, "Tactile-based object center of mass exploration and discrimination," in *Proc. IEEE Int. Conf. Humanoid Robots*, 2017, pp. 876–881.

[21] M. Kaboli, K. Yao, and G. Cheng, "Tactile-based manipulation of deformable objects with dynamic center of mass," in *Proc. IEEE Int. Conf. Humanoid Robots*, 2016, pp. 752–757.

[22] S. J. Lederman, "The perception of surface roughness by active and passive touch," *Bull. Psychonomic Soc.*, vol. 18, pp. 253–255, 1981.

[23] P. Dallaire *et al.*, "Autonomous tactile perception: A combined improved sensing and Bayesian nonparametric approach," *Robot. Auton. Syst.*, vol. 6, pp. 422–435, 2014.

[24] P. Giguere and G. Dudek, "A simple tactile probe for surface identification by mobile robots," *IEEE Trans. Robot.*, vol. 27, pp. 534–544, Jun. 2011.

[25] D. S. Chathuranga, Z. Wang, V. A. Ho, A. Mitani, and S. Hirai, "A biomimetic soft fingertip applicable to haptic feedback systems for texture identification," in *Proc. IEEE Int. Sympo. Haptic Audio Visual Environ. Games*, 2013, pp. 29–33.

[26] N. Jamali and C. Sammut, "Majority voting: Material classification by tactile sensing using surface texture," *IEEE Trans. Robot.*, vol. 27, no. 3, pp. 508–521, Jun. 2011.

[27] A. J. Fishel and G. E. Loeb, "Bayesian exploration for intelligent identification of textures," *Frontiers Neurorobot.*, vol. 6, pp. 1–20, 2012.

[28] J. Sinapov, V. Sukhoy, R. Sahai, and A. Stoytchev, "Vibrotactile recognition and categorization of surfaces by a humanoid robot," *IEEE Trans. Robot.*, vol. 27, no. 3, pp. 488–497, Jun. 2011.

[29] D. Xu, G. E. Loeb, and A. J. Fishel, "Tactile identification of objects using Bayesian exploration," in *Proc. IEEE Int. Conf. Robot. Autom.*, 2013, pp. 3056–3061.

[30] V. Chu *et al.*, "Robotic learning of haptic adjectives through physical interaction," *Robot. Auton. Syst.*, vol. 63, pp. 279–292, 2015.

[31] J. M. Romano *et al.*, "Methods for robotic tool-mediated haptic surface recognition," in *Proc. IEEE Haptics Symp.*, 2014, pp. 49–56.

[32] K. Watanabe *et al.*, "Identification of various kinds of papers using multi-axial tactile sensor with micro-cantilevers," in *Proc. World Hap. Conf.*, Apr. 2013, pp. 139–144.

[33] C. M. Oddo, M. Controzzi, L. Beccai, C. Cipriani, and M. C. Carrozza, "Roughness encoding for discrimination of surfaces in artificial active-touch," *IEEE Trans. Robot.*, vol. 27, no. 3, pp. 522–533, Jun. 2011.

[34] D. Tanaka, T. Matsubara, K. Ichien, and K. Sugimoto, "Object manifold learning with action features for active tactile object recognition," in *Proc. IEEE Int. Conf. Intell. Robots Syst.*, 2014, pp. 516–523.

[35] K. E. Friedl, A. R. Voelker, A. Peer, and C. Eliasmith, "Human-inspired neurorobotic system for classifying surface textures by touch," *IEEE Robot. Autom. Lett.*, vol. 1, no. 1, pp. 516–523, Jan. 2016.

[36] H. Hu *et al.*, "A finger-shaped tactile sensor for fabric surfaces evaluation by 2-dimensional active sliding touch," *Sensors*, vol. 14, pp. 4899–4913, 2014.

[37] A. Song, Y. Han, H. Hu, and J. Li, "A novel texture sensor for fabric texture measurement and classification," *IEEE Trans. Instrum. Meas.*, vol. 63, no. 7, pp. 1739–1747, Jul. 2014.

[38] W. W. Mayol-Cuevas, J. Juarez-Guerrero, and S. Munoz-Gutierrez, "A first approach to tactile texture recognition," in *Proc. IEEE Int. Conf. Syst., Man, Cybern.*, 1998, vol. 5, pp. 4246–4250.

[39] N. H. H. M. Hanif, P. H. Chappell, A. Cranny, and N. M. White, "Surface texture detection with artificial fingers," in *Proc. 37th Annu. Int. Conf. IEEE Eng. Med. Biol. Soc.*, 2015, pp. 8018–8021.

[40] B. Hjorth, "Eeg analysis based on time domain properties," *Electroencephalography Clin. Neurophys.*, vol. 29, pp. 306–310, 1970.

[41] M. Kaboli and G. Cheng, "Novel tactile descriptors and a tactile transfer learning technique for active in-hand object recognition via texture properties," in *Proc. IEEE Int. Conf. Humanoid Robots, Workshop*, Cancun, Mexico, 2016, pp. 1–4.

[42] M. Kaboli and G. Cheng, "Dexterous hands learn to re-use the past experience to discriminate in-hand objects from the surface texture," in *Proc. 33rd Annu. Conf. Robot. Soc.*, 2015, pp. 1–6.

[43] M. Kaboli, P. Mittendorfer, V. Hgel, and G. Cheng, "Humanoids learn object properties from robust tactile feature descriptors via multi-modal artificial skin," in *Proc. IEEE Int. Conf. Humanoid Robots*, 2014, pp. 187–192.

[44] P. Mittendorfer and G. Cheng, "Humanoid multimodal tactile-sensing modules," *IEEE Trans. Robot.*, vol. 27, no. 3, pp. 401–410, Jun. 2011.

[45] S. J. Lederman and R. L. Klatzky, "Haptic perception: A tutorial," *Attention, Perception, Psychophys.*, vol. 71, pp. 1439–1459, 2009.

[46] K. Crammer *et al.*, "Online passive-aggressive algorithms," *J. Mach. Learn. Res.*, vol. 7, pp. 551–585, Dec. 2006.

[47] R.-E. Fan, K.-W. Chang, C.-J. Hsieh, X.-R. Wang, and C.-J. Lin, "Liblinear: A library for large linear classification," *J. Mach. Learn.*, vol. 9, pp. 1871–1874, 2008.

[48] A. P. Dempster, N. M. Laird, and D. B. Rubin, "Maximum likelihood from incomplete data via the em algorithm," *J. Roy. Statist. Soc.*, vol. 39, no. 1, pp. 1–38, 1977.
[49] A. Anil and A. Jain, "Robust data clustering," in *Proc. IEEE Comput. Soc. Conf. Comput. Vision Pattern Recognit.*, 2003, vol. 3, pp. 128–136.
[50] M. Kaboli, K. Yao, D. Feng, P. Lanillos, and G. Cheng, "A tactile-based framework for active object learning and discrimination using multi-modal robotic skin," *IEEE Robot. Autom. Lett.*, vol. 2, no. 4, pp. 2143–2150, Oct. 2017.
[51] M. Kaboli, K. Yao, D. Feng, and G. Cheng, "Tactile-based active object discrimination and target object search in an unknown workspace," *Auton. Robots*, vol. 43, no. 3, pp. 1–30, 2018.
[52] M. Kaboli, D. Feng, and G. Cheng, "Active tactile transfer learning for object discrimination in an unstructured environment using multimodal robotic skin," *Auton. Robots*, vol. 15, no. 1, 2017, Art. no. 1850001.
[53] D. Feng, M. Kaboli, and G. Cheng, "Active prior tactile knowledge transfer for learning tactual properties of new objects," *Sensors*, vol. 18, no. 2, pp. 876–881, 2018.
[54] M. Kaboli, R. Walker, and G. Cheng, "Re-using prior tactile experience by robotic hands to discriminate in-hand objects via texture properties," in *Proc. IEEE Int. Conf. Robot. Autom.*, 2016, pp. 2242–2247.

Mohsen Kaboli received the Bachelor's degree in electrical and electronic engineering and a master's degree in signal processing and machine learning from Royal Institute of Technology (KTH), Stockholm, Sweden, in 2011.

In March 2012, he received a scholarship from the Swiss National Foundation for 18 months to continue his research as a Research Assistant with Idiap Lab, École polytechnique fédérale de Lausanne (EPFL). In April 2013, he was awarded a three-year Marie Curie scholarship. Since that time, he has been with the Institute for Cognitive Systems, the Technical University of Munich (TUM), München, Germany, directed by Prof. G. Cheng. In November 2013, he visited the Shadow Robot Company for two months. He has been a Visiting Researcher with Human Robotics Lab, Department of Bioengineering, Imperial College London from February until April 2014. From September 2015 until January 2016, he spent five months as a Visiting Research Scholar with Intelligent Systems and Informatics Lab, University of Tokyo, Tokyo, Japan.

Gordon Cheng (F'17) received a master degree in Computer Science from the University of Wollongong in Australia, in 1993, and the Ph.D. degree in Systems Engineering from the Australian National University in Australia, in 2001. He is the Professor and the Chair of Cognitive Systems, and Faculty of Electrical and Computer Engineering, Technical University of Munich, Munich, Germany. He is also the Coordinator of the CoC for Neuro-Engineering—Center of Competence Neuro-Engineering, Department of Electrical and Computer Engineering. He is the Speaker of the established Elite Master of Science program in neuroengineering (MSNE) of the Elite Network of Bavaria. Formerly, he was the Head of the Department of Humanoid Robotics and Computational Neuroscience, ATR Computational Neuroscience Laboratories, Kyoto, Japan. He was the Group Leader for the JST International Cooperative Research Project (ICORP), Computational Brain. He has also been a Project Leader/Research Expert with the National Institute of Information and Communications Technology (NICT) of Japan. Recently, he is involved in a large number of major European Union Projects (e.g., Factory-in-a-Day, CONTEST-ITN, RoboCom-Flagship). Over the past ten years, he has been the co-inventor of approximately 20 patents and is the author of approximately 300 technical publications, proceedings, editorials, and book chapters.

Prof. Cheng has been named the IEEE Fellow 2017 for "contributions in humanoid robotic systems and neurorobotics".